

# TE– Mode Solutions for Dielectric Slab Center Loaded Ridged Waveguide

CHARLES W. YOUNG, JR.

*Microwave Techniques Branch  
Electronics Technology Division*

April 29, 1977



**NAVAL RESEARCH LABORATORY**  
**Washington, D.C.**

Approved for public release; distribution unlimited.

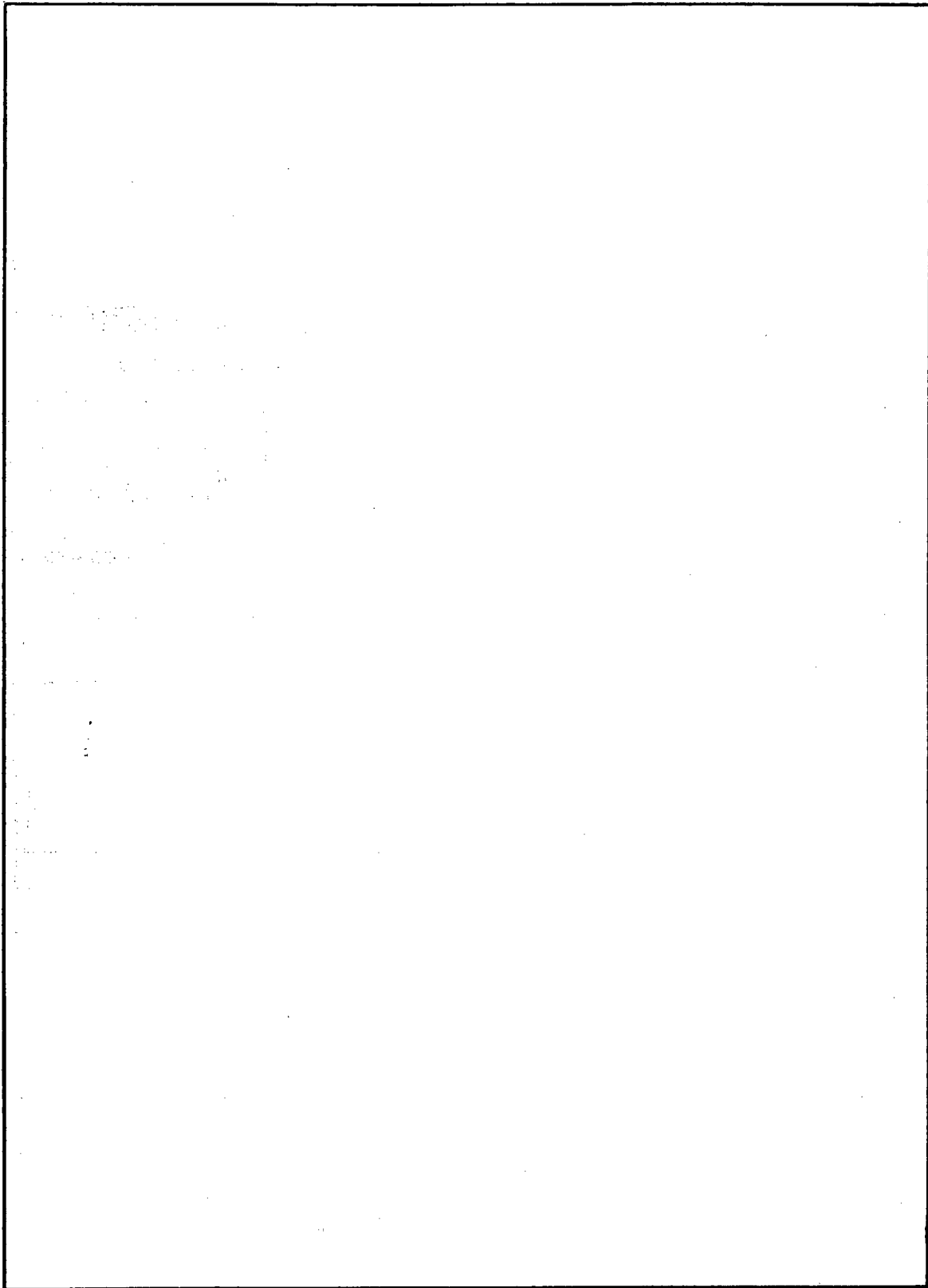
SECURITY CLASSIFICATION OF THIS PAGE (When Data Entered)

REPORT DOCUMENTATION PAGE		READ INSTRUCTIONS BEFORE COMPLETING FORM
1. REPORT NUMBER NRL Report 8105	2. GOVT ACCESSION NO.	3. RECIPIENT'S CATALOG NUMBER
4. TITLE (and Subtitle) TE-MODE SOLUTIONS FOR DIELECTRIC SLAB CENTER LOADED RIDGED WAVEGUIDE		5. TYPE OF REPORT & PERIOD COVERED An interim report on one phase of the NRL problem.
		6. PERFORMING ORG. REPORT NUMBER
7. AUTHOR(s) Charles W. Young, Jr.		8. CONTRACT OR GRANT NUMBER(s)
9. PERFORMING ORGANIZATION NAME AND ADDRESS Naval Research Laboratory Washington, D.C. 20375		10. PROGRAM ELEMENT, PROJECT, TASK AREA & WORK UNIT NUMBERS NRL Problem R06-45H
11. CONTROLLING OFFICE NAME AND ADDRESS Department of the Navy Naval Electronics Systems Command Washington, D.C. 20360		12. REPORT DATE April 29, 1977
		13. NUMBER OF PAGES 18
14. MONITORING AGENCY NAME & ADDRESS (if different from Controlling Office)		15. SECURITY CLASS. (of this report) Unclassified
		15a. DECLASSIFICATION/DOWNGRADING SCHEDULE
16. DISTRIBUTION STATEMENT (of this Report) Approved for public release; distribution unlimited.		
17. DISTRIBUTION STATEMENT (of the abstract entered in Block 20, if different from Report)		
18. SUPPLEMENTARY NOTES		
19. KEY WORDS (Continue on reverse side if necessary and identify by block number) Bandwidth Dielectric loaded Inhomogeneous Ridged waveguide		
20. ABSTRACT (Continue on reverse side if necessary and identify by block number) Dielectric slab center loaded ridged waveguide has been analyzed to obtain $TE_{10}$ propagation characteristics for the lossless case. The analysis was performed by solving for the lowest order resonance of the transverse wave component, using an equivalent transmission line circuit which models the height change at the ridge as an effective shunt susceptance. Calculated and measured data are compared; they show good agreement. The analysis should prove useful in designing transformers to match empty ridged waveguide to slab loaded rectangular waveguide components such as toroidal phase shifters.		

DD FORM 1473  
1 JAN 73EDITION OF 1 NOV 65 IS OBSOLETE  
S/N 0102-LF-014-6601

i

SECURITY CLASSIFICATION OF THIS PAGE (When Data Entered)



## CONTENTS

INTRODUCTION .....	1
BACKGROUND .....	1
ANALYSIS .....	2
CONCLUSION .....	8
REFERENCES .....	9
APPENDIX A - Equivalent Circuit for a Change in Height of Rectangular Waveguide .....	10
APPENDIX B - Fortran Listing of Computer Program .....	12

## TE-MODE SOLUTIONS FOR DIELECTRIC-SLAB CENTER-LOADED RIDGED WAVEGUIDE

### INTRODUCTION

Applications exist which require dielectric or ferrite slab center loaded rectangular waveguide to be used in conjunction with ridged waveguide. Transitions can be made with stepped matching transformers; these transformers are appropriate sections of a composite of the two different waveguide configurations. The objective of this report is to present an analysis of such dielectric slab center loaded ridged waveguide and to provide a method of obtaining equations for the  $TE_{n,0}$  propagation characteristics, thus facilitating transformer design.

### BACKGROUND

Because higher order modes can easily cause mismatch and transmission loss spikes, waveguide operation is generally limited to a frequency band where only the principal mode may propagate. Conventional rectangular waveguide has a theoretical two-to-one, or single octave, principal-mode-only frequency bandwidth; in practice, the useable bandwidth is less because of large attenuation near the cut-off frequency.

Ridged waveguide, particularly double-ridged waveguide, is commonly used when larger bandwidths are required at high power levels. A frequency range of more than four to one between the cut-off frequencies of the  $TE_{10}$  and  $TE_{20}$  modes can easily be obtained [1,2] using double-ridged waveguide. Similar bandwidths can be obtained with dielectric slab center loaded rectangular waveguide [3,4,5]. Both ridged and slab loaded waveguide achieve broad bandwidths by adding large capacitance to the dominant mode while only slightly affecting the capacitance of the next higher order mode.

Ferrite toroidal phase shifters also can be designed for operation in excess of one octave. Because of the small gap spacing of ridged waveguide, the phase shifters are generally made in rectangular waveguide. Dielectric slab center loaded rectangular waveguide would be readily compatible with the ferrite toroidal phase shifter, but it is not a commonly used transmission line. Since ridged waveguide is commonly used, it would be desirable to have compatibility, i.e., matching transitions, between ridged waveguide and ferrite toroidal loaded rectangular waveguide. Dielectric loaded tapered transitions are possible, but the fabrication would be very difficult. Also, a quasi-Tchebycheff transformer design should give better matching for given length transitions. The latter approach requires transformer sections of dielectric loaded ridged waveguide, but analysis of this type of transmission line is not currently available in the literature. The analysis in this report employs an equivalent transmission line circuit for the transverse component of the propagating electromagnetic wave to derive solutions for the  $TE_{n,0}$  propagation constants in such waveguide.

## ANALYSIS

TE-mode solutions for the dielectric slab center loaded rectangular waveguide of Fig. 1a can be derived by using ABCD matrices [6] or by using an equivalent transmission line circuit for the crossguide component of the electromagnetic wave. The homogeneous double-ridged waveguide of Fig. 1b has been analyzed [1,2] by using the latter method in conjunction with the equivalent discontinuity susceptance due to the height change at the ridge wall.

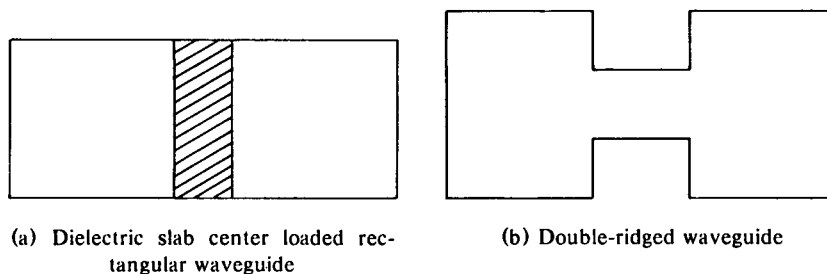


Fig. 1 — Broadband waveguide cross sections

For the dielectric slab center loaded double ridged waveguide of Fig. 2, the analysis is similar to that for the homogeneous case, with an extra section incorporated in the equivalent transmission line circuit. The dimensions referred to in all subsequent calculations are those shown in Fig. 2. For simplicity, this report will consider only the case for  $TE_{n0}$  modes and will assume that the transmission line is lossless, i.e., perfectly conducting waveguide walls and a dielectric loss tangent of zero. Axial symmetry will also be assumed.

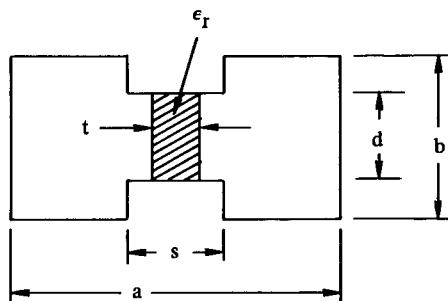


Fig. 2 — Cross section of dielectric slab center loaded, double-ridged waveguide

Cohn's article on ridged waveguide [2] points out that for the homogeneous case (i.e.  $\epsilon_r = 1$ ) the cross section may be treated at the cut-off frequency by assuming that it is an infinitely wide, composite, parallel strip transmission line short-circuited at two points. The resultant electromagnetic field may be considered as an electromagnetic wave traveling from side to side without longitudinal propagation. The resonant conditions can then be solved for the cut-off frequencies of the different  $TE_{n0}$  modes.

A similar argument holds for the inhomogeneous case. In addition, the longitudinal propagation constant may be treated as the unknown quantity, and solutions at any frequency may be obtained by separating the wave vector in each region into its transverse and longitudinal components. Since the waveguide configuration is symmetrical, the resonance condition for the transverse wave component will result in an infinite (zero) impedance at the center for  $n$  odd (even). Half of a cross section is shown in Fig. 3a, and the equivalent transmission line circuits

for the transverse wave are shown in Fig. 3b for  $n$  odd and Fig. 3c for  $n$  even. Since the equivalent circuit is a composite, dissipationless, passive line matched at both ends, it is matched at all points. Therefore, the sum of the admittances at the plane  $y_2$  of the effective lumped capacitance due to the ridge wall must equal zero. Within each region, where the regions are shown in Fig. 3a,  $Z_{0i}$  is the characteristic impedance,  $Y_{0i} = 1/Z_{0i}$  is the characteristic admittance, and  $\theta_i$  is the transverse electrical length;  $\theta_i$  is equal to the product of the physical transverse dimension of the region and  $\gamma_{yi}$ , the complex transverse propagation constant. Since all regions are lossless,  $\gamma_{yi}$ , and therefore  $\theta_i$ , will be purely real or purely imaginary.

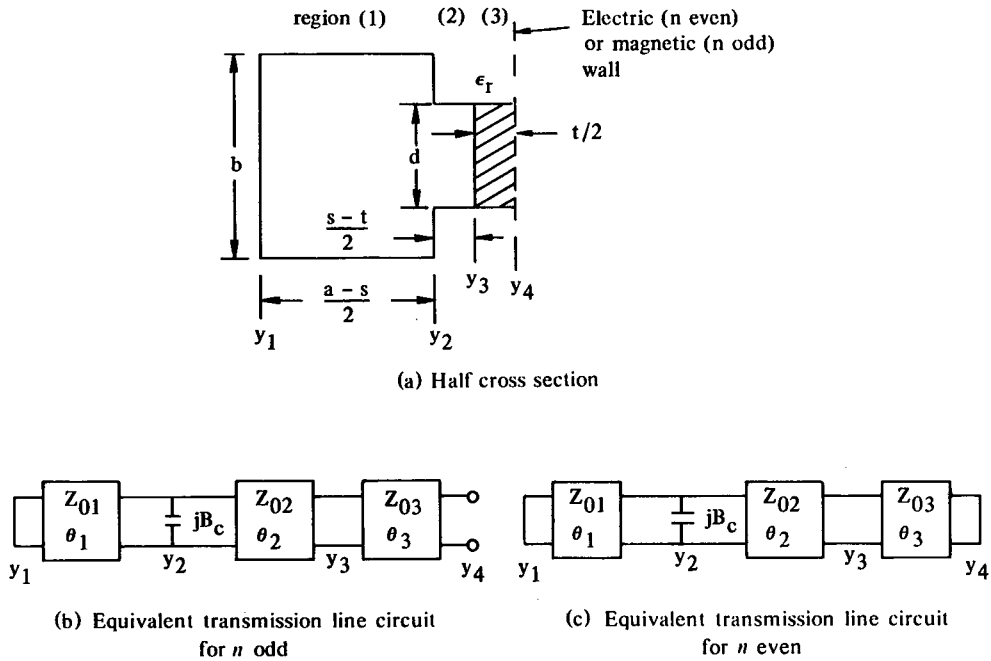


Fig. 3 — Half waveguide cross section and equivalent transmission line circuits for transverse wave

The reflected impedance  $Z$  presented by a load impedance  $Z_L$  terminating a transmission line of characteristic impedance  $Z_0$  with propagation constant  $\gamma$  and length  $w$  is [7]

$$Z = Z_0 \frac{(Z_L + Z_0)e^{\gamma w} + (Z_L - Z_0)e^{-\gamma w}}{(Z_L + Z_0)e^{\gamma w} - (Z_L - Z_0)e^{-\gamma w}} \quad (1)$$

The short circuit at  $y_1$  in Fig. 3b will be reflected back to  $y_2$  as  $Z_{1-2}$  where

$$Z_{1-2} = Z_{01} \tanh \left[ \gamma_{y1} \frac{a-s}{2} \right] \quad (2)$$

or

$$Y_{1-2} = \gamma_{01} \coth \left[ \gamma_{y1} \frac{a-s}{2} \right] \quad (3)$$

The open circuit at  $y_4$  will reflect back to  $y_3$  as  $Z_{4-3}$  with

$$Z_{4-3} = Z_{03} \coth \left[ \gamma_{y3} \frac{t}{2} \right]. \quad (4)$$

Equation (1) can be rewritten in the form

$$Z = Z_0 \frac{Z_L \cosh \gamma w + Z_0 \sinh \gamma w}{Z_L \sinh \gamma w + Z_0 \cosh \gamma w}. \quad (5)$$

Since  $Z_{4-3}$  terminates region 2,

$$Z_{4-2} = Z_{02} \frac{Z_{4-3} \cosh \left[ \gamma_{y2} \frac{s-t}{2} \right] + Z_{02} \sinh \left[ \gamma_{y2} \frac{s-t}{2} \right]}{Z_{4-3} \sinh \left[ \gamma_{y2} \frac{s-t}{2} \right] + Z_{02} \cosh \left[ \gamma_{y2} \frac{s-t}{2} \right]}. \quad (6)$$

Using  $\theta_i = \gamma_{yi} w_i$  to simplify notation and substituting Eq. (4) into Eq. (6) yields

$$Z_{4-2} = Z_{02} \frac{Z_{03} \coth \theta_3 \cosh \theta_2 + Z_{02} \sinh \theta_2}{Z_{03} \coth \theta_3 \sinh \theta_2 + Z_{02} \cosh \theta_2} \quad (7)$$

or

$$Y_{4-2} = Y_{02} \frac{Z_{03} \coth \theta_3 \sinh \theta_2 + Z_{02} \cosh \theta_2}{Z_{03} \coth \theta_3 \cosh \theta_2 + Z_{02} \sinh \theta_2}. \quad (8)$$

Since the sum of admittances at  $y_2$  must equal zero,

$$Y_{1-2} + jB_c + Y_{4-2} = 0. \quad (9)$$

Substituting Eqs. (3) and (8) into Eq. (9) yields

$$Y_{01} \coth \theta_1 + jB_c + Y_{02} \frac{Z_{03} \coth \theta_3 \sinh \theta_2 + Z_{02} \cosh \theta_2}{Z_{03} \coth \theta_3 \cosh \theta_2 + Z_{02} \sinh \theta_2} = 0 \quad (10)$$

or

$$\coth \theta_1 + j \frac{B_c}{Y_{01}} + \frac{Y_{02}}{Y_{01}} \frac{\coth \theta_3 \sinh \theta_2 + \frac{Z_{02}}{Z_{03}} \cosh \theta_2}{\coth \theta_3 \cosh \theta_2 + \frac{Z_{02}}{Z_{03}} \sinh \theta_2} = 0. \quad (11)$$

Since region 1 and region 2 have the same propagation constant,  $\gamma_{y1} = \gamma_{y2}$ , the impedances are proportional to the heights:

$$\frac{Z_{02}}{Z_{01}} = \frac{Y_{01}}{Y_{02}} = \frac{d}{b}. \quad (12)$$

Regions 2 and 3 have equal heights, and since the transverse wave is  $TE$ , the impedance ratio is

$$\frac{Z_{02}}{Z_{03}} = \frac{\gamma_{y3}}{\gamma_{y2}}. \quad (13)$$

The left side of Eq. (11) may be rewritten as a single fraction. All terms in the denominator are finite, so the numerator may be equated to zero. The resultant expression is

$$\left[ \frac{b}{d} \sinh \theta_1 \right] [\gamma_{y2} \cosh \theta_3 \sinh \theta_2 + \gamma_{y3} \sinh \theta_3 \cosh \theta_2] + \left[ \cosh \theta_1 + j \frac{B_c}{Y_{01}} \sinh \theta_1 \right] \\ \times [\gamma_{y2} \cosh \theta_3 \cosh \theta_2 + \gamma_{y3} \sinh \theta_3 \sinh \theta_2] = 0. \quad (14)$$

Within each region,

$$\gamma_{xi}^2 + \gamma_{yi}^2 + \gamma_{zi}^2 = -\omega^2 \mu_0 \epsilon_i \quad (15)$$

where

$$\begin{aligned} \epsilon_i &= \epsilon_0 \text{ for } i = 1, 2 \\ &= \epsilon_r \epsilon_0 \text{ for } i = 3. \end{aligned}$$

For  $TE$  modes,  $\gamma_{xi} = 0$  for all regions and  $\gamma_{zi} = j\beta$  for all regions;  $\beta$  is the longitudinal propagation constant (above cutoff) for the waveguide configuration. Substituting

$$\begin{aligned} \gamma_{yi} &= \sqrt{\beta^2 - \omega^2 \mu_0 \epsilon_i} \text{ for } \omega^2 \mu_0 \epsilon_i < \beta^2 \\ &= j\sqrt{\omega^2 \mu_0 \epsilon_i - \beta^2} \text{ for } \omega^2 \mu_0 \epsilon_i \geq \beta^2 \end{aligned} \quad (16)$$

and

$$\theta_i = \gamma_{yi} w_i$$

with

$$\begin{aligned} w_1 &= 1/2 (a - s) \\ w_2 &= 1/2 (s - t) \\ w_3 &= 1/2 t \end{aligned} \quad (17)$$

into Eq. (14) yields the transcendental equation in  $\beta$  that must be solved for  $TE_{n0}$  ( $n$  odd) modes. The smallest root of Eq. (14) is the  $TE_{10}$  solution, the next root the  $TE_{30}$  solution, etc.

For  $TE_{n0}$  ( $n$  even) modes, the analysis starts with the equivalent transmission line circuit of Fig. 3b and proceeds in a manner similar to the case for  $n$  odd. The resultant transcendental equation is

$$\left[ \frac{b}{d} \sinh \theta_1 \right] [\gamma_{y2} \sinh \theta_3 \sinh \theta_2 + \gamma_{y3} \cosh \theta_3 \cosh \theta_2] + \left[ \cosh \theta_1 + j \frac{B_c}{Y_{01}} \sinh \theta_1 \right] \\ \times [\gamma_{y2} \sinh \theta_3 \cosh \theta_2 + \gamma_{y3} \cosh \theta_3 \sinh \theta_2] = 0 \quad (18)$$

with Eqs. (16) and (17) being applicable.

If  $\epsilon_r = 1$ , it is straightforward to show that Eqs. (14) and (18) reduce to the expressions for the odd and even mode cutoff frequencies, respectively, for double-ridged waveguide [1,2]. Also, if  $b = d$ ,  $B_c$  equals zero and Eqs. (14) and (18) result in expressions for the odd- and even-mode propagation constants of dielectric slab center loaded rectangular waveguide identical to those obtained by use of ABCD matrices [6].

The discontinuity-susceptance term  $B_c/Y_{01}$  is obtained from the *Waveguide Handbook* [8]. Appendix A gives the necessary equations for calculating  $B_c/Y_{01}$  in terms of the waveguide dimensions (from Fig. 2) and the effective wavelength  $\lambda_g$ . Note that  $\lambda_g$  is the wavelength of the wave component which is incident normal to the height change. Therefore  $\lambda_g$  of Appendix A is the wavelength of the transverse wave in regions 1 and 2, namely  $\lambda_{y1}$ .

For standard (i.e. air filled) double-ridged waveguide  $\epsilon_r = 1$ ; thus

$$\gamma_{y1} = \gamma_{y2} = \gamma_{y3} = j\beta_y$$

and  $\lambda_{yi} = 2\pi/\beta_y$  is a real constant for a given configuration. However, for the general case  $\epsilon_r > 1$  and

$$\gamma_{y1} = \gamma_{y2} \neq \gamma_{y3},$$

with the result that the values of  $\gamma_{yi}$  that satisfy Eq. (14) or (18), subject to (16) and (17), are no longer constant but depend on the frequency. This is of course to be expected, since for any nonhomogeneous waveguide a  $1/\sqrt{1 - (f_{c/f})^2}$  term no longer describes the dispersive nature. However, there is another problem because of the inhomogeneity. At all frequencies above cutoff, the transverse wave propagation constant in the dielectric region will be entirely imaginary; i.e.,

$$\gamma_{y3} = j\beta_{y3} \text{ for } \omega > \omega_c.$$

However, there is a critical frequency  $\omega_{crit}$  ( $\omega_{crit}$  is greater than the cutoff frequency  $\omega_c$ ; how much greater depends upon the degree of dielectric loading) such that for frequencies greater than  $\omega_{crit}$  the transverse propagation constant in regions 1 and 2 is real, that is,

$$\gamma_{y1} = \gamma_{y2} = \alpha_{y1} \text{ for } \omega > \omega_{crit}.$$

When  $\omega > \omega_{crit}$ , the transverse "wave" in these regions is no longer a resonant traveling wave but rather the fields are decaying exponentially away from the dielectric region, and the concept of wavelength in the region of the discontinuity is not meaningful. The expression for the  $B_c/Y_{01}$  term from Ref. 8 is no longer applicable; indeed, the validity of the equivalent transmission line circuit for the waveguide height change (a shunt susceptance at the junction of two transmission lines of unequal characteristic impedance) is questionable for operation below cutoff. Also, the calculation for  $B_c/Y_{01}$  is based on a model which assumes that the waveguide extends to infinity in both directions away from the height discontinuity; in practice, the assumption is valid if additional mismatches are far enough removed from the height discontinuity so that the local fields have decayed to small proportions. These local fields are the evanescent modes of the fringing fields caused by the height discontinuity, and they decay very rapidly.

Future investigation is planned to model an equivalent circuit of the waveguide height change to include operation below as well as above the cut-off frequency, and to include the proximity effects of waveguide walls and dielectric center loading. However, for this report the following two engineering assumptions are made:

1. The  $B_c/Y_{01}$  term can be neglected for frequencies below the critical frequency. Since

$$\frac{B_c}{Y_{01}} \rightarrow 0 \text{ as } \omega \rightarrow \omega_{crit}^{(+)}$$

and for  $\omega < \omega_{crit}$  the fields of the transverse wave are decaying exponentially in the region of the height discontinuity, a small shunt susceptance term will have only a minor effect on the solution for  $\beta$ . Equations (14) and (18) are transcendental equations and must be solved by some algorithm using trial values of  $\beta$ . If a trial value of  $\beta$  yields an imaginary transverse propagation constant in region 1, the  $B_c/Y_{01}$  term is calculated with

$$\gamma_{y1} = j\beta_{y1} \text{ and } \lambda_{y1} = \frac{2\pi}{\beta_{y1}}.$$

If the trial value of  $\beta$  results in  $\gamma_{y1}$  real, the  $B_c/Y_{01}$  term is neglected, i.e. set equal to zero, in Eqs. (14) and (18).

2. Proximity effects can be neglected in the calculation of  $B_c/Y_{01}$ .

Although the validity of these two assumptions may be questioned from a rigorous theoretical aspect, the close agreement between calculated and measured values of  $\beta$  for different configurations (shown in Figs. 4 and 5) indicates that both assumptions result in accuracy sufficient for most practical applications.

A listing of a computer program to solve for the principal ( $TE_{10}$ ) mode propagation constant of dielectric slab center loaded double-ridged waveguide is given in Appendix B.

All discussions and calculations thus far have assumed a double-ridged waveguide configuration. For the asymmetric or single-ridged waveguide configurations shown in Fig. 6, Eqs. (14) and (18) remain valid; however, the expression for  $B_c/Y_{01}$  must have  $\lambda_{y1}$  replaced by  $1/2 \lambda_{y1}$ .

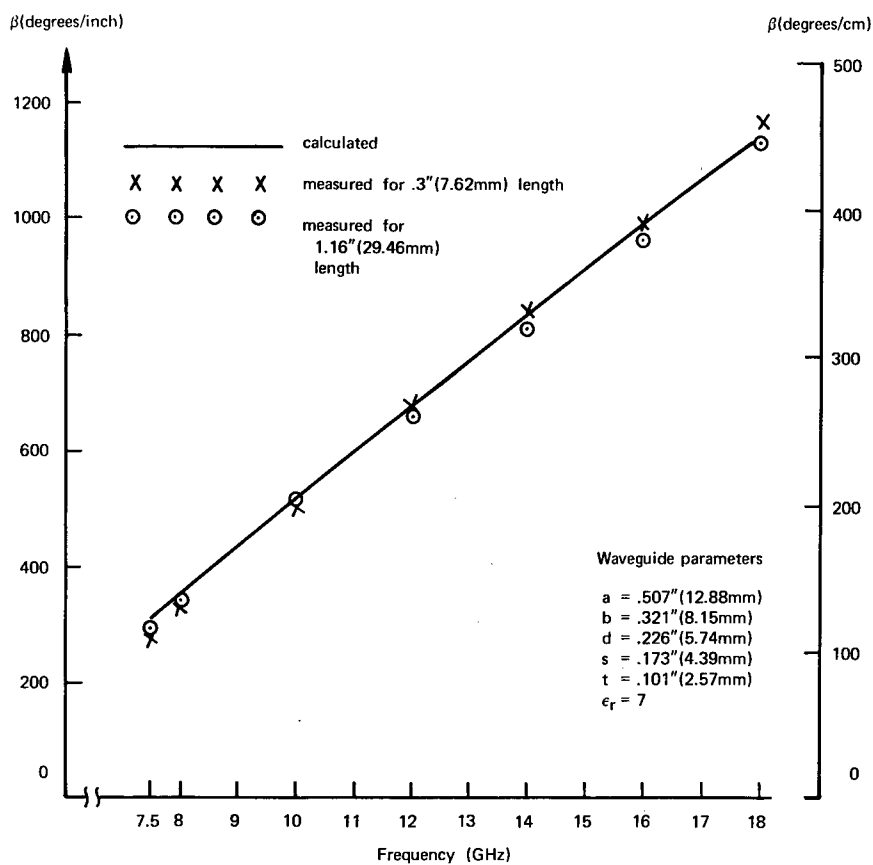


Fig. 4 — Calculated and measured values of  $\beta$  for dielectric slab loaded double-ridged waveguide

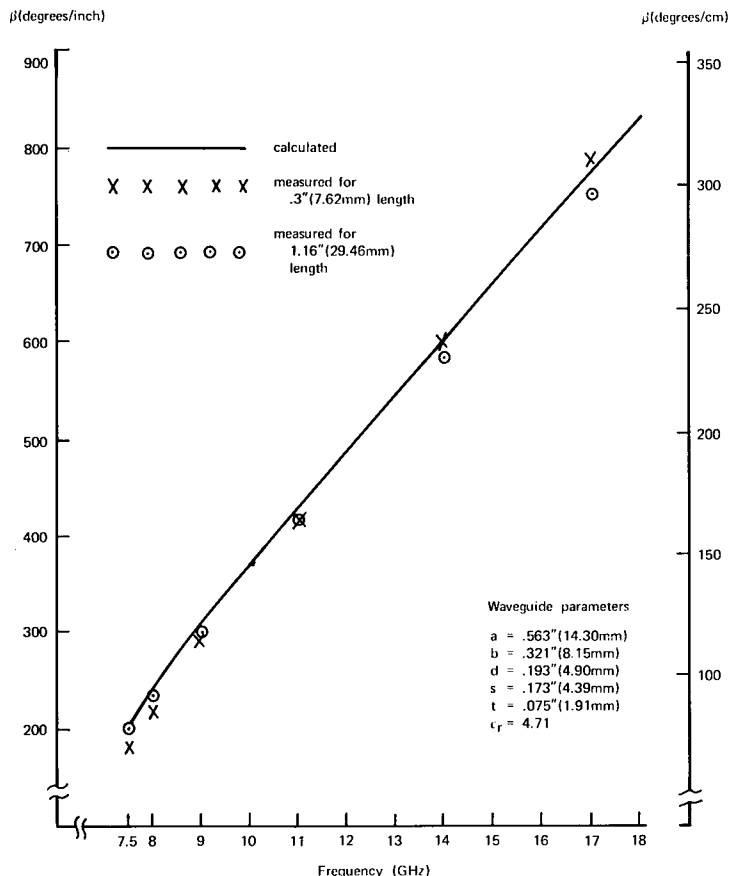


Fig. 5 — Calculated and measured values of  $\beta$  for dielectric slab loaded doubled-ridged waveguide

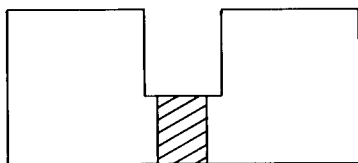


Fig. 6 — Cross section of dielectric slab center loaded single-ridged waveguide

### CONCLUSION

Based on the equivalent transmission line circuit for the transverse component of the propagating electromagnetic wave, expressions have been derived for the  $TE_{n0}$  mode propagation constants of a dielectric slab center loaded ridged waveguide configuration. These expressions are transcendental equations involving the propagation constant, but they can readily be solved with a computer. Based on the agreement between calculated and measured data, certain assumptions made in the derivation appear valid. The analysis should prove useful in designing transformers to match ridged waveguide to dielectric or ferrite slab center loaded rectangular waveguide.

## REFERENCES

1. S. Hopfer, "The Design of Ridged Waveguides," *IRE Trans. MTT-3* (5), 20-29 (Oct. 1955).
2. S. B. Cohn, "Properties of Ridge Wave Guide," *Proc. IRE*, **35**, 783-788 (Aug. 1947).
3. P. H. Vartanian, W. P. Ayres, and A. L. Helgesson, "Propagation in Dielectric Slab Loaded Rectangular Waveguide," *IRE Trans. MTT-6*, 215-222 (April 1958).
4. T. K. Findakly and H. M. Haskal, "On the Design of Dielectric Loaded Waveguides," *IEEE Trans. MTT-24*, 39-43 (Jan. 1976).
5. R. Seckelmann, "Propagation of TE Modes in Dielectric Loaded Waveguides," *IEEE Trans. MTT-14*, 518-527 (Nov. 1966).
6. W. P. Clark, K. H. Hering, and D. A. Charlton, "TE-Mode Solutions for Partially Ferrite Filled Rectangular Waveguide Using ABCD Matrices," *IEEE International Convention Record*, **14** (Mar. 1966).
7. W. C. Johnson, *Transmission Lines and Networks*, McGraw-Hill, New York, 1950.
8. N. Marcuvitz, *Waveguide Handbook*, MIT Radiation Laboratory Series, McGraw-Hill, New York, 1951.

## Appendix A EQUIVALENT CIRCUIT FOR A CHANGE IN HEIGHT OF RECTANGULAR WAVEGUIDE

For a height change of rectangular waveguide as shown in Figs. A1a and A1b, the equivalent circuit given by the *Waveguide Handbook*\* is shown in Fig. A1c. The characteristic admittances of the different height waveguides are  $Y_0$  and  $Y'_0$ ,  $T$  is the effective terminal plane,  $B_c$  is the effective shunt capacitive susceptance, and  $\lambda_g$  is the wavelength of the propagating wave. The admittance ratio is

$$\frac{Y_0}{Y'_0} = \frac{d}{b} = \alpha$$

and at the terminal plane  $T$

$$\frac{B_c}{Y_0} = \frac{2b}{\lambda_g} \left\{ \ln \left( \frac{1 - \alpha^2}{4\alpha} \right) + \frac{1}{2} \left( \alpha + \frac{1}{\alpha} \right) \ln \left( \frac{1 + \alpha}{1 - \alpha} \right) + 2 \frac{A + A' + 2C}{AA' - C^2} + \left( \frac{b}{4\lambda_g} \right)^2 \left( \frac{1 - \alpha}{1 + \alpha} \right)^{4\alpha} \left( \frac{5\alpha^2 - 1}{1 - \alpha^2} + \frac{4}{3} \frac{\alpha^2 C}{A} \right) \right\}$$

where

$$A = \left( \frac{1 + \alpha}{1 - \alpha} \right)^{2\alpha} \frac{1 + \sqrt{1 - \left( \frac{b}{\lambda_g} \right)^2}}{1 - \sqrt{1 - \left( \frac{b}{\lambda_g} \right)^2}} - \frac{1 + 3\alpha^2}{1 - \alpha^2}$$

$$A' = \left( \frac{1 + \alpha}{1 - \alpha} \right)^{2/\alpha} \frac{1 + \sqrt{1 - \left( \frac{d}{\lambda_g} \right)^2}}{1 - \sqrt{1 - \left( \frac{d}{\lambda_g} \right)^2}} + \frac{3 + \alpha^2}{1 - \alpha^2}$$

and

$$C = \left( \frac{4\alpha}{1 - \alpha^2} \right)^2.$$

The equivalent circuit is valid for  $b/\lambda_g < 1$ .

\*N. Marcuvitz, *Waveguide Handbook*, MIT Radiation Laboratory Series, McGraw-Hill, New York, 1951.

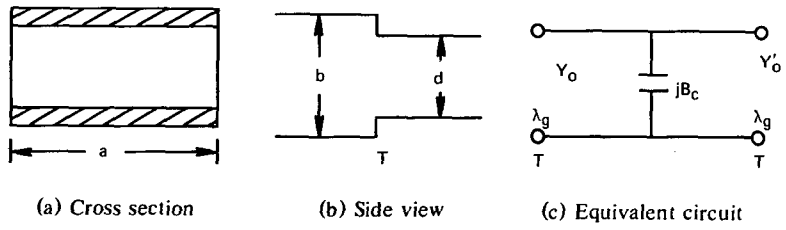


Fig. A-1 — Height change of rectangular waveguide and equivalent circuit

## Appendix B

### FORTRAN LISTING OF COMPUTER PROGRAM

```

00100  C THIS IS PROGRAM DRWGDL.FOR - CWY -OCT 75
00200      INTEGER RIK
00300      REAL KXAIR
00400      PI=3.1415927
00500      C=2.997925E+08
00600      R1=39.37008
00700      R2=2.0*R1
00800      RRNDI=180.0/(PI*R1)
00900      C1=(2.0E+09*PI/C)**2
01000      NEWRUN=0
01100      TYPE 600
01200  600  FORMAT (//// PROGRAM DRWGDL/CWY/OCT 75/// COMPUTES
01300  1 TE10 CUTOFF FREQUENCIES AND PROPAGATION CONSTANTS OF//
01400  2 / SYMMETRIC DIELECTRIC LOADED DOUBLE RIDGED WAVEGUIDE/)
01500  105  TYPE 605
01600  605  FORMAT (/// WAVEGUIDE DIMENSIONS IN INCHES - A,B,D,S: ($)
01700      READ(5,*)A,B,D,S
01800  106  TYPE 615
01900  615  FORMAT (/ RELATIVE DIELECTRIC CONSTANT OF CENTER
02000  1 LOADING = ($)
02100      READ(5,*)EPSR
02200      TYPE 625
02300  625  FORMAT (/ WIDTH IN INCHES OF CENTER LOADING = ($)
02400      ACCEPT 630,T
02500  630  FORMAT (F8.3)
02600      IF(T.LT.S)GO TO 108
02700      TYPE 631
02800  631  FORMAT (/ DIELECTRIC WIDTH MUST BE LESS THAN
02900  1 RIDGE WIDTH ---- TRY AGAIN/)
03000      GO TO 105
03100  108  TYPE 606
03200  *606  FORMAT (/// DRWGDL PARAMETERS ----- DIMENSIONS IN
03300  1 INCHES//8X/ A/9X/ B/9X/ D/9X/ S/12X/ T/6X4HEPS//1X$)
03400      TYPE 607,A,B,D,S,T,EPSR
03500  607  FORMAT (4F10.4,F13.4,F10.3)
03600      R=D/B
03700      RS=R**2
03800      IFR=0
03900      IF (ABS(R-1.0).LT.1.0E-06) IFR=1
04000      W1=(A-S)/R2
04100      W2=(S-T)/R2
04200      W3=T/R2
04300      CEREST=1.+(1./R-1.)*COS(PI*(A-S)/(2.*A))
04400      CLREST=CEREST+(EPSR-1.)/R*COS(PI*(A-T)/(2.*A))
04500      EDCTRY=CLREST/CEREST
04600      ALCEST=A*CLREST*(R+(1.-R)*SIN(PI*(A-S)/(2.*A)))
04700  C THE ABOVE FOUR QUANTITIES ARE TO BE USED FOR CALCULATING
04800  C APPROXIMATE (STARTING VALUES) OF CUTOFF FREQUENCIES AND
04900  C PROPAGATION CONSTANTS
05000      IBC=1

```

```

05100      FREQ=C*R1/(ALCEST*2.0E+09)
05200      DELBY=0.31*FREQ
05300      BY=0.0
05400      GO TO 112
05500  109   IF (NEWRUN.LT.2) GO TO 210
05600      IF (FSTART.GT.FCGHZ) GO TO 220
05700  210   TYPE 635
05800  635   FORMAT (// FREQUENCIES IN GHZ - START,STOP,INCREMENT: ($)
05900      READ(5,*) FSTART,FSTOP,DELFI
06000  640   FORMAT (F9.3,1X,F9.3,1X,F9.3)
06100  220   IF (FSTART.LT.1.0E-13) GO TO 180
06200      IF (FSTART.GT.FCGHZ) GO TO 230
06300      TYPE 645
06400  645   FORMAT ( FREQUENCY MUST BE GREATER THAN CUTOFF )
06500      GO TO 210
06600      IF (FSTOP.LT.1.0E-13) FSTOP=FSTART-1.0
06700  230   TYPE 655
06800  655   FORMAT (/4X4HFREQ08X4HBETA9X3HGWL7X5HRATIO8X5HKXAIR/
06900  1 5X3HGHZ6X6HDEG/IN6X6HINCHES4X8HGWL/FSWL7X6HR OR I/)
07000  110   IFREQ=0
07100      FREQ=FSTART
07200  111   IFREQ=IFREQ+1
07300      BY=PI*2.E+09/C*SQRT(EDCTRY*(FREQ**2+FCGHZ**2))
07400  C THIS IS A FIRST TRY FOR BETA
07500      DELBY=-0.31*BY
07600  112   ICROSS=0
07700      ITAN=0
07800      IBTRY=0
07900  115   C1F=C1*FREQ**2
08000      C1FEP=C1F*EPSR
08100  120   IBTRY=IBTRY+1
08200      IF (IBTRY.LT.26) GO TO 122
08300      TYPE 705
08400  705   FORMAT ( MORE THAN 25 TRIES AT ROOT )
08500      GO TO 170
08600  122   BYSQ=BY**2
08700      GX3SQ=C1FEP-BYSQ
08800      GX2SQ=C1F-BYSQ
08900      GX3=SQRT (ABS (GX3SQ))
09000      GX2=SQRT (ABS (GX2SQ))
09100      IF (GX3SQ) 130,132,132
09200  130   CHS3=SINH (GX3*W3)
09300      CHC3=COSH (GX3*W3)
09400      IRGX3=1
09500      GO TO 134
09600  132   CHS3=SIN (GX3*W3)
09700      CHC3=COS (GX3*W3)
09800      IRGX3=-1
09900  134   CONTINUE
10000      IF (GX2SQ) 136,138,138

```

```

10100 136   CHS2=SINH (GX2+M2)
10200      CHC2=COSH (GX2+M2)
10300      CHS1=SINH (GX2+M1)
10400      CHC1=COSH (GX2+M1)
10500      KXAIR=GX2
10600      RIK=1HR
10700      IRGX2=1
10800      GO TO 140
10900 138   CHS2=SIN (GX2+M2)
11000      CHC2=COS (GX2+M2)
11100      CHS1=SIN (GX2+M1)
11200      CHC1=COS (GX2+M1)
11300      IRGX2=-1
11400      KXAIR=GX2+RRMDI
11500      RIK=1HI
11600 140   BOY=0.0
11700      IF (IFR.EQ.1) GO TO 153
11800      IF (IRGX2.EQ.1) GO TO 153
11900  C CALCULATE B/Y TERM
12000      P=(1+R)/(1-R)
12100      GL=2.0+PI/GX2
12200      P2=SQRT (1.0-(B/(R1+GL))**2)
12300      P3=SQRT (1.0-(D/(R1+GL))**2)
12400      PA=P** (2.0+R) + (1.0+P2)/(1.0-P2) - (1.0+3.0+RS)/(1.0-RS)
12500      PAP=P** (2.0/R) + (1.0+P3)/(1.0-P3) + (3.0+RS)/(1.0-RS)
12600      PC=((4.0+R)/(1.0-RS))**2
12700      PT1=ALOG ((1.0-RS)/(4.0+R) + P** (0.5+(R+1.0/R)))
12800      PT2=2.0+(PA+PAP+2.0+PC)/(PA+PAP-PC**2)
12900      PT3=(B/(R1+4.0+GL))**2+(1.0/P)** (4.0+R) + ((5.0+RS
13000 1 -1.0)/(1.0-RS) + 4.0+RS+PC/(3.0+PA))**2
13100      BOY=2.0+B*(PT1+PT2+PT3)/(R1+GL)
13200  C CALCULATE F (BETA)
13300 153   FBETA=R*(-BOY+CHS1+CHC1) + (GX2/GX3+CHC3+CHC2
13400 1 +IRGX3+CHS3+CHS2) + IRGX2+CHS1 + (GX2/GX3+CHC3+CHS2
13500 2 +IRGX2+IRGX3+CHS3+CHC2)
13600      IF (IBC.EQ.1) BY=FREQ
13700  C ROOT SEARCH ROUTINE
13800      IF (ABS (FBETA) .LT. 1.0E-08) GO TO 170
13900      IF (IBTRY.EQ.1) GO TO 163
14000      IF (ITAN.EQ.1) GO TO 164
14100      IF (FBETA+FBOLD.LT.0.0) GO TO 161
14200      IF (ABS (FBETA) .GT. ABS (FBOLD)) DELBY=-DELBY
14300      GO TO 162
14400 161   DELBY=-DELBY
14500      ICROSS=1
14600 162   IF (ICROSS.EQ.1) DELBY=0.5+DELBY
14700 163   BYNEW=BY+DELBY
14800      IF (ABS ((BY-BYNEW)/BY) .LT. 0.1) ITAN=1
14900      GO TO 166
15000 164   IF (ABS (BY-BYOLD) .LT. 1.E-05 .AND. FBETA.LT. 1.E-06) GO TO 170

```

```

15100      BYNEW=BY-FBETA*(BY-BYOLD)/(FBETA-FBOLD)
15200  166      BYOLD=BY
15300      BY=BYNEW
15400      FBOLD=FBETA
15500      IF(IBC.EQ.2)GO TO 120
15600      FREQ=BY
15700      BY=0.0
15800      GO TO 115
15900  170      IF(IBC.EQ.2)GO TO 175
16000      FCGHZ=BY
16100      TYPE 658,FCGHZ,BOY
16200  658      FORMAT(// TE10 MODE CUTOFF FREQUENCY IN GHZ = 'F7.4'
16300  1        B/Y = 'F7.3)
16400      IBC=2
16500      GO TO 109
16600  173      CONTINUE
16700  175      BYDI=BY*RRMDI
16800      GWL=360.0/BYDI
16900      FSWL=R1*D/(FREQ*1.0E+09)
17000      RGLFS=GWL/FSWL
17100  177      TYPE 660,FREQ,BYDI,GWL,RGLFS,KXAIR,RIK
17200  660      FORMAT (1X,F7.3,3X,F9.2,3X,F9.4,4X,F8.4,3X,F8.2,1X,A1)
17300      IF(FREQ.GE.FSTOP)GO TO 180
17400      FREQ=FREQ+DELF
17500      GO TO 111
17600  180      TYPE 665
17700  665      FORMAT (/// WISH NEW PARAMETERS? NONE=0, ALL=1,
17800  1        CENTER LOADING=2, FREQ=3      ($)
17900      ACCEPT 670,NEWRUN
18000  670      FORMAT (I1)
18100      GO TO(199,105,106,210,180)NEWRUN+1
18200  199      CONTINUE
18300      END

```

parameters of  $k = 1 - 2\pi$  (0.000124) and  $G = 100$  is shown in Figs. 4 and 5. Although the LMS algorithm had unstable performance, the improved algorithm had completely stable performance. Also, for slow loops there will be ringing in the LMS algorithm, which will result in degraded cancellation performance. In a previous paper Kretschmer\* investigated cascading sidelobe canceler stages as a method of obtaining improved cancellation ratios and transient responses. Thus a higher effective loop gain would be achieved with low actual loop gains, which are required for stable operation. In lieu of their later work, the improved algorithm provides another way of obtaining high loop gains. Lewis and Kretschmer are now working on an open-loop digital implementation of a sidelobe canceler.

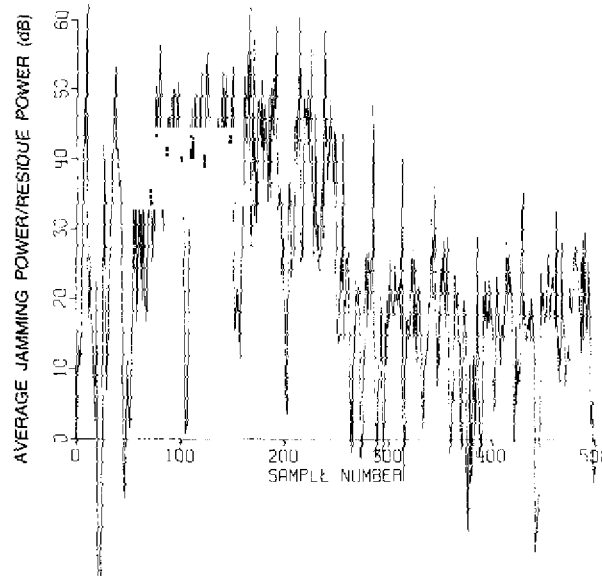


Fig. 4 — Adaptive-canceler response of the LMS algorithm

The sidelobe canceler removes the jamming signal after it has entered the main antenna. Adaptive arrays, which require individual receiving elements, attempt to prevent jamming from entering the antenna receive pattern by placing a receiving antenna null in the direction of the jammer. Before commencing with a discussion of adaptive arrays and radars, it is pointed out that the September 1976 issue of the IEEE Transactions on Antennas and Propagation is a special issue on adaptive arrays and contains many interesting articles.

#### Adaptive Arrays and Radars

Qualitatively, in an adaptive array the received signal is the weighted sum of the signal at the individual receiving elements, with the weights being a function of the received signal. The theory of adaptive arrays was first discussed by Applebaum,<sup>†</sup> and Widrow et al.<sup>‡</sup> have

\*F. F. Kretschmer, IEEE International Radar Conf., 181-185, 1975.

†S. P. Applebaum, "Adaptive arrays," Syracuse University Research Corp. Report SPL-769, June 1964.

‡B. Widrow, P. E. Mantey, L. J. Griffiths, and B. B. Goode, Proc. IEEE 55, 2143-2159 (1967).

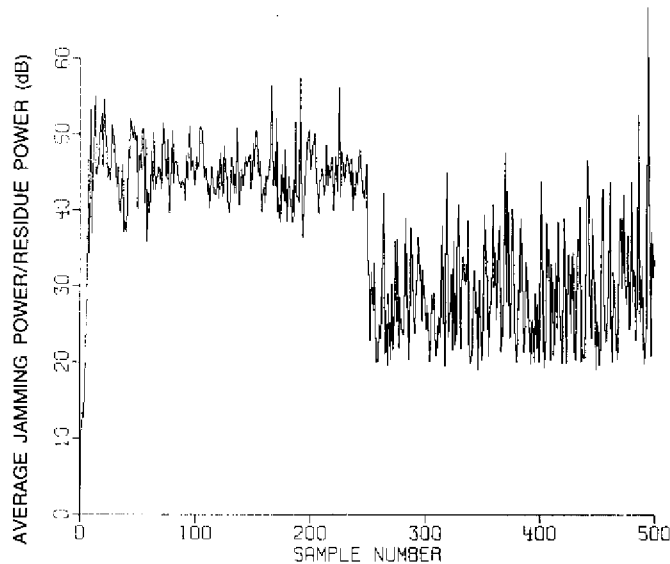


Fig. 5 — Adaptive canceler response of the Kretschmer-Lewis algorithm

made major contributions to the theory; however a later development of Brennan and Reed\* will be followed. Their approach is similar to Applebaum's in that they maximize  $S/N$ , which they show is equivalent to maximizing the probability of detection when the noise is Gaussian distributed.

Let the radar be composed of  $N$  receiving elements, and let the last  $M$  time samples from each element be processed. Thus there are  $n = NM$  space-time samples. Define  $S$  to be a complex (amplitude and phase)  $n$ -vector which contains the desired signal components, and define  $X$  to be a complex  $n$ -vector containing the noise samples. The radar return  $Z$  is given by

$$Z = S + X. \quad (17)$$

To detect the signal  $S$ , the radar output is passed through a linear filter described by a weighting vector  $W$ . Thus the output of the detector (the filter) is

$$Y = W^T Z. \quad (18)$$

Brennan and Reed showed that  $S/N$  at the output of the filter is

$$\left( \frac{S}{N} \right)_o = \frac{|W^T S|^2}{W^T K W}, \quad (19)$$

where the asterisk indicates the complex conjugate and  $K$  is the noise covariance matrix,  $K = E\{X^* X^T\}$ ,  $X$  having zero mean. Consequently what is required is the value of  $W$  that maximizes (19). If the Schwarz inequality is used, it can be shown that the maximum value of (19) is  $S^T K^{-1} S^*$  and that this value is obtained when

$$W = a' K^{-1} S^*, \quad (20)$$

\*L. E. Brennan and I. S. Reed, IEEE Trans. Aerospace and Electronic Systems AES-9, 237-252 (1973).

where  $a'$  is an arbitrary nonzero complex number. This criterion has been known for some time.\* However, it is rarely used, since  $K$  is not known a priori; and if  $K$  is estimated, it has been extremely difficult to invert  $K$  in real time.

What makes the Brennan-and-Reed approach different from other adaptive array processing is not the ability to place spatial nulls in the direction of jammers but rather the temporal processing that is equivalent to a motion-compensated MTI (moving-target indicator). The compensated MTI behavior is obtained by selecting the proper steering signal  $S$ . The selection of the steering signal  $S$  will be illustrated for the case of an airborne coherent pulsed radar.

Assume that the return is range gated, there are  $N_R$  range cells, and the return from the  $j$ th cell is

$$Z(j) = X(j) + S(j). \quad (21)$$

The return signal from the  $r$ th receiving element and  $m$ th time sample can be written as

$$S_r(m) = b_r e^{im\gamma}, \quad r = 1, \dots, N, \quad (22)$$

where  $\gamma = -4\pi VT/\lambda$  is the doppler phase shift, with  $V$  being the relative velocity of the target,  $T$  being the time between transmitted pulses, and  $\lambda$  being the radar wavelength. The quantity  $b_r$  is

$$b_r = A_r e^{i\phi_r + i\delta}, \quad r = 1, \dots, N, \quad (23)$$

where  $A_r$  is the signal amplitude at the  $r$ th element,  $\delta$  is a constant phase factor, and  $\phi_r$  is the relative phase between the target and the  $r$ th element. For a linear array with element spacing  $d$ , the phase angles  $\phi_r$  for a signal arriving at an angle  $\psi$  with respect to the array normal are

$$\phi_r = \frac{2\pi rd}{\lambda} \sin \psi, \quad r = 1, \dots, N. \quad (24)$$

Thus the expected signal for a linear array can be obtained by substituting (23) and (24) into (22).

Both clutter and target will have returns of the form of (22). Since the velocity of the target (and consequently the relative velocity  $V$ ) is unknown, it is impossible to specify  $S$  for the optimal weighting given by (20). However, since (22) is computable for ground clutter as a function of the radar-clutter-cell geometry, one selects a *steering* signal  $S$  which is orthogonal to the ground-clutter vector  $S'$ . Thus the purpose of  $S$  is to reject the clutter, not to detect the target. This is about as close to an optimal detector as one can obtain, since it can be shown\* that no uniform most-powerful test exists when the target velocity is unknown.

As an example let  $M = 2$  and assume one wants to detect a target in a direction normal to the direction of the platform velocity (the radar is sidelooking). Then  $S_r(m) = A_r e^{i\delta}$ , and for uniform amplitude taper ( $A_r = 1$ ,  $r = 1, \dots, N$ ) the clutter signal is

$$S'^T = e^{i\delta} [1, \dots, 1, 1, \dots, 1]. \quad (25)$$

The appropriate steering signal  $S$  which is orthogonal to  $S'$ ,  $S'^T S'^* = 0$ , is

$$S^T = [1, \dots, 1, -1, \dots, -1]. \quad (26)$$

\*H. L. VanTrees, IEEE Trans. Military Electronics **MIL-9**, 216-229 (1965).

which corresponds to a target at 1/2 the blind speed of the radar:

$$V = \frac{1}{2} \left( \frac{\lambda}{2T} \right). \quad (27)$$

Thus, if (26) is used in (20), the detector is optimized for canceling main-beam clutter. We now consider how (20) can be implemented adaptively.

Brennan and Reed use the method of steepest ascent to maximize S/N:

$$F \triangleq \frac{|W^T S|^2}{W^T K W}. \quad (28)$$

The recursive algorithm for steepest ascent is

$$W(j+1) = W(j) + \frac{1}{2} \mu(j) \nabla F[W(j)], \quad (29)$$

where  $\nabla F[W(j)]$  is the complex gradient of  $F$  evaluated at  $W(j)$ , which has been shown to be

$$\nabla F = 2 \left[ \frac{W^T S}{W^T K W} \right] \left[ S^* - \left[ \frac{W^T S^*}{W^T K W} \right] K W \right]. \quad (30)$$

If  $K$  is assumed known and  $\mu(j)$  is chosen to be a constant, one can apply known theorems\* to show  $W(j)$  approaches a critical point as a limit. Thus, if  $W(0)$  is sufficiently close to the optimal value,  $W(j)$  approaches  $a'K^{-1}S^*$  in the limit.

The trouble with using (30) in (29) is that  $\nabla F$  is a nonlinear function of  $W(j)$ , which in some adaptive systems can cause computational difficulties. Hence the algorithm was linearized by noting

$$\lim_{j \rightarrow \infty} \frac{W^T S}{W^T K W} = \frac{1}{a'} \triangleq a. \quad (31)$$

Thus, if  $\mu(j)$  equals a constant  $\mu$ , (29) reduces to

$$W(j+1) = W(j) + \mu a [S^* - a'K(j)W(j)], \quad (32)$$

where  $K(j)$  is a statistical estimate of the unknown covariance matrix  $K$ . The best (maximum-likelihood) estimate of  $K$  is

$$K(j) = Z^*(j)Z^T(j). \quad (33)$$

Brennan and Reed then showed that (32) converged. Specifically, the expected value of (32) converges to  $a'\bar{K}^{-1}S^*$ , where  $\bar{K} = E\{K(j)\}$  for all  $j$ , if  $Z(j)$  are independent and  $0 < \mu < 2a'^2/\max \lambda_i$ , where  $\lambda_i$  ( $i = 1, \dots, n$ ) are the eigenvalues of  $\bar{K}$ .

The block diagram of the adaptive radar is shown in Fig. 6, and the implementation of an adaptive loop is shown in Fig. 7. The steady-state antenna pattern can be calculated from (20), and the S/N improvement can be found from  $S^T K^{-1} S^*$ . However in many radar environments the clutter has a temporal and spatial variation; consequently the rate of convergence is important. To study this phenomena, computer simulations were used.

\*M. J. D. Powell, SIAM Rev. 12, 79-97 (1970).

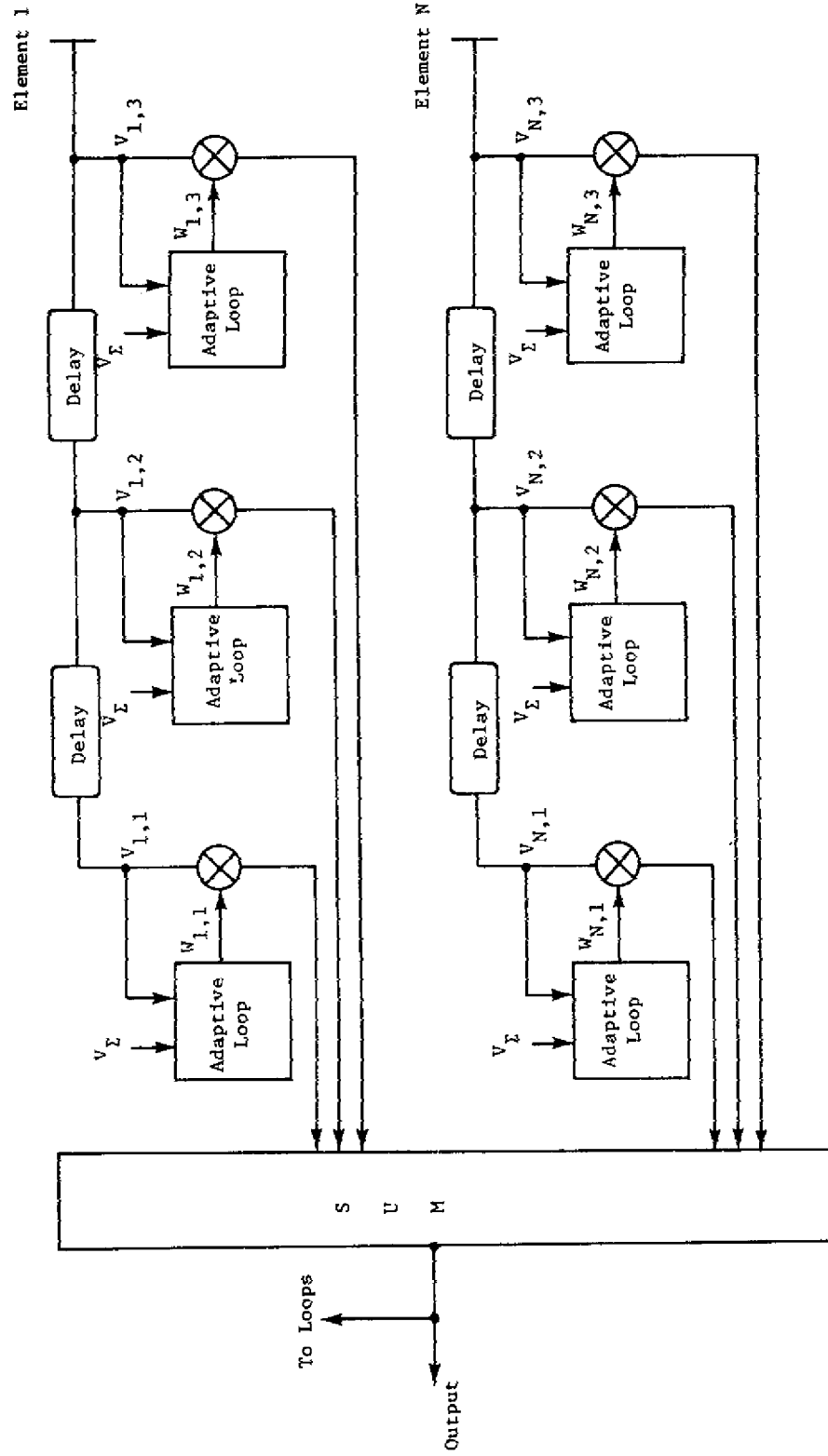


Fig. 6 — Adaptive AMTI radar using control loops. (From L. E. Brennan, J. D. Mallett, and I. S. Reed, IEEE Trans. Antennas and Propagation AP-24, 607-615 (1976), courtesy of the Institute of Electrical and Electronics Engineers.)

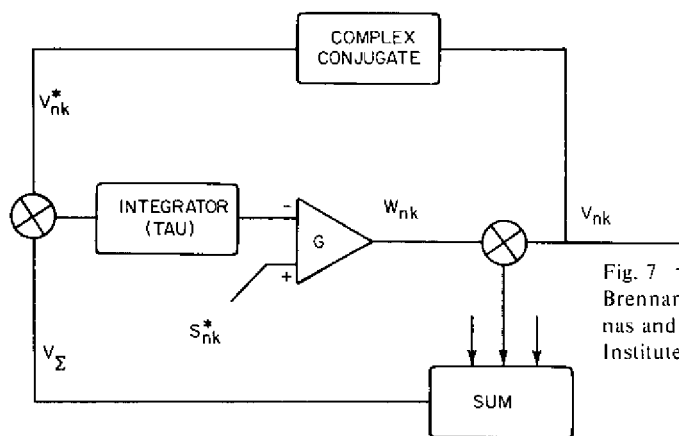


Fig. 7 -- Implementation of an adaptive loop. (From L. E. Brennan, J. D. Mallett, and I. S. Reed, IEEE Trans. Antennas and Propagation AP-24, 607-615 (1976), courtesy of the Institute of Electrical and Electronics Engineers.)

The basic parameters for a ten-element adaptive array using only one time sample ( $N = 10$  and  $M = 1$ ) are given in Table 1. In the first simulation, 30 discrete clutter points were uniformly distributed in the two symmetrical intervals  $[17^\circ, 90^\circ]$  and  $[-17^\circ, -90^\circ]$ , and the radar was looking normal to the aircraft velocity vector. The simulation results are summarized in Fig. 8, where the base of the plot is 45 dB below the peak gain. The back antenna pattern is the initial receiving pattern, the middle eight patterns are from range cells 200 to 1600 in 200 range-cell intervals, and the last pattern is the steady-state pattern. Since there are 30 interference sources and only 10 elements, it is impossible to put a null at each interference angle. Rather the adaptive array follows two strategies: it widens the main beam and consequently lowers the general sidelobe level, and it places receiver nulls at transmitter maximums and vice versa. After 1600 interactions all but 1.6 dB (27.3 - 25.7) of the maximum signal-to-clutter improvement has been obtained.

In the second simulation the 30 clutter points were placed nonsymmetrically about zero in the interval  $[15^\circ, 45^\circ]$ . The simulation results are summarized in Fig. 9. Although the sidelobes are reduced in the proper angular interval, after 1600 iterations only 24.7 dB of the possible 44.1-dB improvement in the signal-to-clutter ratio has been obtained. Brennan and Reed have shown that the time behavior of the weights is a sum of exponentials of the form

$$W_i = \sum_{k=1}^N C_{ik} e^{[-(G\lambda_k + 1)t/\tau]}, \quad (34)$$

where  $\tau$  is the time constant and  $G$  is the gain of the low-pass filter. Thus the rate of convergence is controlled by the smallest eigenvalue of  $K$ ; specifically, the effective time constant is  $\tau/(G\lambda_{\min} + 1)$ . This suggests that rapid convergence can be obtained by selecting  $G$  to be large and/or  $\tau$  to be small. However this is not a useful solution to the convergence problem, since Brennan et al.\* have shown that the total output noise power in the adaptive array is

$$P = \mathbf{W}^T \mathbf{K} \mathbf{W} \left( 1 + \frac{G}{2\tau} \sum_{l=1}^N \lambda_l \right), \quad (35)$$

\*L. E. Brennan, E. L. Pugh, and I. S. Reed, IEEE Trans. Aerospace and Electronic Systems AES-7, 254-262 (1971).

Table 1 — Parameters Assumed in a  
Simulation of an Adaptive Receiving Array

Ten-element linear array  
 Element patterns isotropic over  $-\pi/2 \geq \nu \leq \pi/2$   
 Half-wave-spaced elements  
 Uniformly illuminated transmit array  
 30 scatterers in the sidelobe region, equally spaced in angle  
 No interference for  $-\theta_1 < \theta < \theta_1$   
 Each receiving-element weight controlled adaptively  
 Simulation of 1600 independent sets of input signals (range  
 resolution cells)  
 No receiver noise

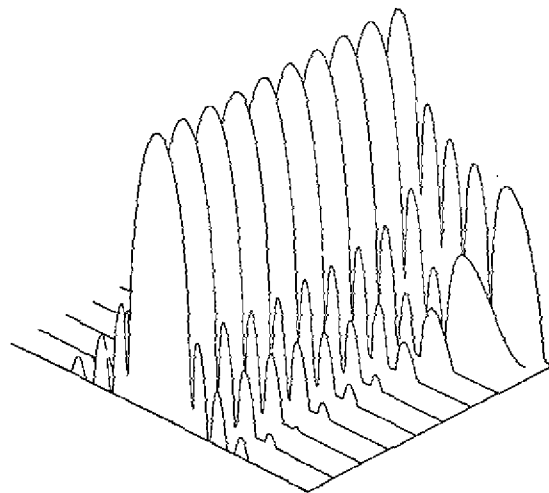
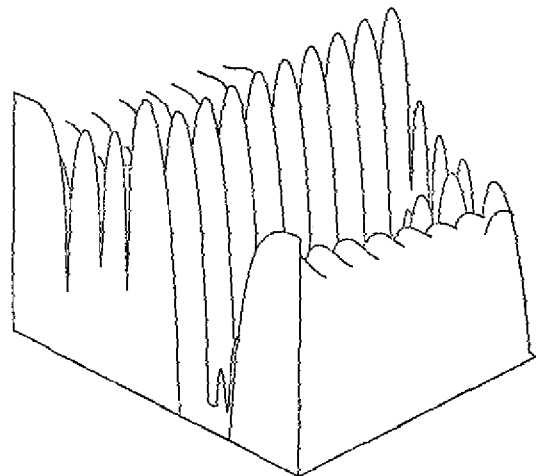


Fig. 8 — Projectograph plot of the gain of a ten-element adaptive array in the case of symmetric clutter distribution. The improvement in the signal-to-sidelobe clutter ratio from the initial receiving pattern (at the rear) is 27.3 dB for steady state (pattern at the front) and 25.7 dB after 1600 iterations. (From L. E. Brennan and L. S. Reed, IEEE Trans. Aerospace and Electronic Systems **AES-9**, 237-252 (1973), courtesy of the Institute of Electrical and Electronics Engineers.)

Fig. 9 — Projectograph plot of the gain of a ten-element adaptable array in the case of nonsymmetric clutter distribution. The improvement in the signal-to-sidelobe clutter ratio is 44.1 dB for steady state (not shown) and 24.7 dB after 1600 iterations (pattern at the front). (From L. E. Brennan and L. S. Reed, IEEE Trans. Aerospace and Electronic Systems **AES-9**, 237-252 (1973), courtesy of the Institute of Electrical Engineers.)



where  $\mathbf{W}$  is the average weight vector in the absence of loop noise (departure from steady state). The quantity  $\mathbf{W}^T \mathbf{K} \mathbf{W}$  is the noise power when  $\mathbf{W} = \mathbf{K}^{-1} \mathbf{S}^*$ . Consequently, the output power has been increased by the factor  $G \Sigma \lambda_r / 2\tau$  due to loop noise. Thus, when  $\mathbf{K}$  contains both small and large eigenvalues, it is impossible to select a  $G$  and  $\tau$  which yield both rapid convergence and low loop noise. To avoid the convergence problem, Reed et al.\* have suggested a direct computation of the weights.

The maximum-likelihood estimate of  $\mathbf{K}$ , assuming the noise is Gaussian distributed, is

$$\hat{\mathbf{K}} = \frac{1}{L} \sum_{j=1}^L \mathbf{Z}^*(j) \mathbf{Z}^T(j). \quad (36)$$

Since  $\mathbf{Z}^*(j) \mathbf{Z}^T(j)$  is an  $n$ -by- $n$  matrix of rank 1,  $L$  must be  $\geq n$  for the inverse to exist. Then the filter has the form

$$\hat{\mathbf{W}} = \hat{\mathbf{K}}^{-1} \mathbf{S}^*. \quad (37)$$

The output S/N for (37) normalized by the maximum S/N,  $\mathbf{S}^T \mathbf{K}^{-1} \mathbf{S}^*$ , which corresponds to (20), is

$$\rho(\hat{\mathbf{K}}) = \frac{(\mathbf{S}^T \hat{\mathbf{K}}^{-1} \mathbf{S}^*)^2}{(\mathbf{S}^T \mathbf{K}^{-1} \mathbf{S}^*) (\mathbf{S}^T \hat{\mathbf{K}}^{-1} \mathbf{K} \hat{\mathbf{K}}^{-1} \mathbf{S}^*)}. \quad (38)$$

The expected value of (38) is

$$E\{\rho(\hat{\mathbf{K}})\} = (L + 2 - n) / (L + 1). \quad (39)$$

Thus the average loss can be kept less than 3 dB ( $E\{\rho(\hat{\mathbf{K}})\} \geq 1/2$ ) by letting  $L \geq 2n$ .

However, whereas the adaptive loops of Fig. 6 require  $n$  complex multiplications, the sample-matrix inverse method requires approximately  $n^3$  complex multiplications. To reduce the complexity of the method, one can update the covariance matrix using

$$\hat{\mathbf{K}}_j = (1 - \alpha) \hat{\mathbf{K}}_{j-1} + \alpha \mathbf{Z}^*(j) \mathbf{Z}^T(j), \quad (40)$$

where  $\alpha$  is the weight applied to the current sample. Then the inverse of  $\hat{\mathbf{K}}_j$ , given  $\hat{\mathbf{K}}_{j-1}$ , is†

$$\hat{\mathbf{K}}_j^{-1} = \frac{\hat{\mathbf{K}}_{j-1}^{-1}}{1 - \alpha} - \left[ \frac{\alpha}{1 - \alpha} \right] \frac{\left[ \hat{\mathbf{K}}_{j-1}^{-1} \mathbf{Z}^*(j) \right] \left[ \mathbf{Z}^T(j) \hat{\mathbf{K}}_{j-1}^{-1} \right]}{(1 - \alpha) + \alpha \mathbf{Z}^T(j) \hat{\mathbf{K}}_{j-1}^{-1} \mathbf{Z}^*(j)}. \quad (41)$$

This method of updating the inverse requires approximately  $2n^2$  complex multiplications. The average computation time for updating the weights  $\mathbf{W}$  depends on how frequently they must be updated. For example, depending on the radar environment, updating the weights every PRF using (36) may be quite adequate; consequently the computation time may be less than that of the adaptive loops.

Brennan et al.‡ compared the convergent rates of the three methods using a computer simulation illustrating airborne MTI performance. The results of the simulation are shown in

\*I. S. Reed, J. D. Mallett, and L. E. Brennan, IEEE Trans. Aerospace and Electronics Systems **AES-10**, 853-863 (1974).

†J. M. Shapard, D. Edelblute, and G. Kinnison, Naval Undersea Research and Development Center Report NUC-TN-528, May 1971.

‡L. E. Brennan, J. D. Mallett, and I. S. Reed, IEEE Trans. Antennas and Propagation **AES-24**, 607-615 (1976).

Fig. 10. In both instances, (a) forward looking and (b) sidelooking, the two methods of calculating  $\hat{K}^{-1}$  provide an excellent convergent rate. Figure 10 indicates an MTI gain of plus 100 dB, but in practice the MTI gain would be limited to a lower figure by internal clutter motion.

Most work on adaptive arrays and radars has been limited to theoretical studies. However there has been some experimental work at Ohio State University,\* the Naval Research Laboratory,† and the Wide-Aperture HF Radio Research Facility operated by Stanford Research Institute.‡§

### Moving-Target Indicators

Moving-Target Indicators (MTIs) were first investigated in the 1940's, and they have been discussed in detail in the books by Skolnik## and Nathanson††. The coherent MTI, the most common MTI, uses an internal coherent reference source to distinguish a moving target from fixed clutter returns. The MTI signal is obtained by coherently subtracting the returned voltages from successive transmitted pulses:

$$Z'_i(j) = Z_i(j) - Z_{i-1}(j), \quad (42)$$

where  $Z_i(j)$  is the  $i$ th returned pulse in the  $j$ th range cell. Larger clutter attenuations can be obtained by using multiple pulses. The frequency (doppler) response of the MTI is that of a bandpass filter.

The most serious problems associated with MTI are limiting and blind speeds. The first of these can be covered very simply. In the classic paper of Ward and Shrader‡‡ it was shown that MTI improvement could be degraded by 20 dB in a three-pulse canceler by limiting the clutter return. Their work showed that the degradation was fundamental to limiting and that consequently a large dynamic range is required to avoid limiting.

The major problem with MTI is that blind speeds, corresponding to doppler frequencies higher than Nyquist rate, occur at

$$V_B = \frac{\ell\lambda}{2T}, \quad \ell = 1, 2, 3, \dots \quad (43)$$

Thus for an L-band (1.3-GHz) radar with a PRF of 300 pps the blind speeds occur at multiples of approximately 70 knots. Because of the width of the clutter notch (rejection region of the canceler), many air targets would not be detected. There are several solutions to the problem

\*R. T. Compton, IEEE Trans. Antennas and Propagation AP-24, 697-706 (1976).

†W. F. Gabriel, "Proceedings Adaptive Antenna Systems Workshop March 11-13, Vol. 1", NRL Report 7803, Sept. 1974.

‡L. J. Griffiths, IEEE Trans. Antennas and Propagation AP-24, 707-720 (1976).

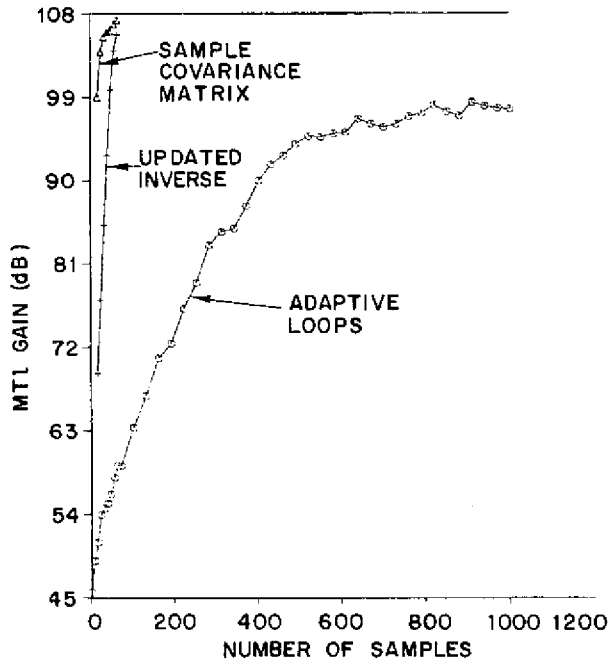
§T. W. Washburn and L. E. Sweeney, Jr., IEEE Trans. Antennas and Propagation AP-24, 721-732 (1976).

# M. I. Skolnik, *Introduction to Radar Systems*, McGraw-Hill, New York, 1962.

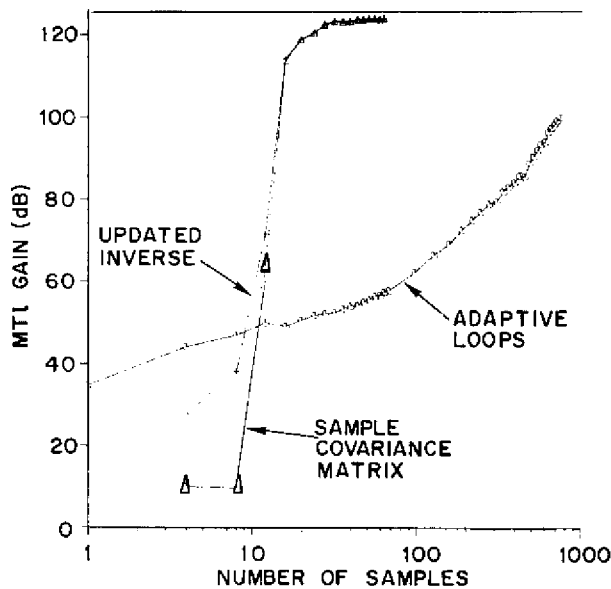
\*\*M. I. Skolnik, editor *Radar Handbook*, McGraw-Hill, New York, 1970.

††F. E. Nathanson, *Radar Design Principles*, McGraw-Hill, New York, 1969.

‡‡H. R. Ward and W. W. Shrader, EASCON Convention Record, 168-173, 1968.



(a) Scan angle = 0.0° and steady-state gain = 108.1 dB



(b) Scan angle = 90.0° and steady-state gain = 125.5 dB

Fig. 10 — Adaptive performance as a function of the number of samples (eight elements, two pulses, element spacing = 0.5, interpulse motion = 0.2). (From L. E. Brennan, J. D. Mallett, and I. S. Reed, IEEE Trans. Antennas and Propagation AP-24, 607-615 (1976), courtesy of the Institute of Electrical and Electronics Engineers.)

# Survey of Radar Signal Processing

G. V. TRUNK

*Radar Analysis Staff  
Radar Division*

June 21, 1977



**NAVAL RESEARCH LABORATORY**  
Washington, D.C.

Approved for public release; distribution unlimited.

of blind speeds in MTIs. Among these are variable PRF, staggered-PRF MTI, and dual-frequency MTI.

The simplest solution is to use a variable-PRF system. If an interpulse period of  $T$  is used, a blind speed of  $V_B$  is obtained. Then, if the interpulse period is changed by a small fraction  $r$ , the blind speed changes by the same fraction  $r$ ; and the smallest common blind speed is  $V_B/(1 - r)$ . Thus, if an L-band radar has two PRFs, 300 pps and 270 pps, the blind speed of the radar system is approximately 700 knots. There are two disadvantages of such a system: (a) second-time-around clutter (clutter beyond the unambiguous range, caused by ducting at sea or high-altitude long-range clutter such as mountains and chaff) passes through the MTI, and (b) the constant PRF for a two- or three-pulse burst makes the system more vulnerable to jamming. The simple solution to (a), using an extra filler pulse (transmitting three pulses but only using the last pulse out of a two-pulse MTI), makes situation (b) worse.

An elegant solution to the blind-speed problem is the staggered-PRF MTI. The basic MTI configuration is shown in Fig. 11. The interpulse durations  $\tau_i$  are constrained by the relation

$$F_B \tau_i = \ell_i, \quad (44)$$

where  $F_B$  is the first blind doppler frequency and  $\ell_i$  are integers for all  $i$ . Capon\* showed that the optimal weights  $\{a_i\}$  for minimizing the output clutter residue while retaining some fraction of the average gain of the filter (this constraint avoids the trivial solution  $a_i = 0$ , for all  $i$ ) are the components of the eigenvector associated with the smallest eigenvalue of the clutter covariance matrix. This procedure ignores what happens in the filter passband. Hsiao and Kretschmer† developed a procedure for setting the interpulse periods to minimize the RMS passband ripple while maintaining the minimum clutter residue. A typical response is shown in Fig. 12. The basic trouble with this system is that second-time-around clutter will not be canceled.

A third solution to the blind-speed problem is the dual-frequency MTI first discussed by Kroszczyński‡§ and later by Hsiao#. The system works by transmitting two frequencies whose ratio  $r$  is slightly less than 1, filtering out the sum signal and retaining the difference signal. The system performance is basically that of a low-frequency radar; hence the blind-speed problem is reduced. The detrimental factor is that the clutter improvement factor is reduced by several dB. A typical filter response for a dual-frequency MTI is shown in Fig. 13. Although the passband response is quite variable, no attempt has been made to reduce the variation by changing  $r$ . Hsiao indicates that the staggered-PRF MTI is preferable to the dual-frequency MTI. However this author believes that the dual-frequency MTI should not be discarded that readily. An alternate solution, and possibly a better one, is to operate individual MTIs at the two frequencies.

\*J. Capon, IEEE Trans. Information Theory **IT-10**, 152-159 (1964).

†J. K. Hsiao and F. F. Kretschmer, Jr., The Radio and Electronic Engineer **43**, 689-693 (1973).

‡J. Kroszczyński, Radio and Electronic Engineer **34**, 157-159 (1967).

§J. Kroszczyński, Radio and Electronic Engineer **39**, 172-176 (1970).

#J. K. Hsiao, The Radio and Electronic Engineer **45**, 351-356 (1975).

Fig. 11 — A staggered-PRF MTI filter.  
 (From J. K. Hsiao and F. F. Kretschmer, *Radio and Electronic Engineer* **43**, 689-693 (1973), courtesy of the Institution of Electronic and Radio Engineers.)

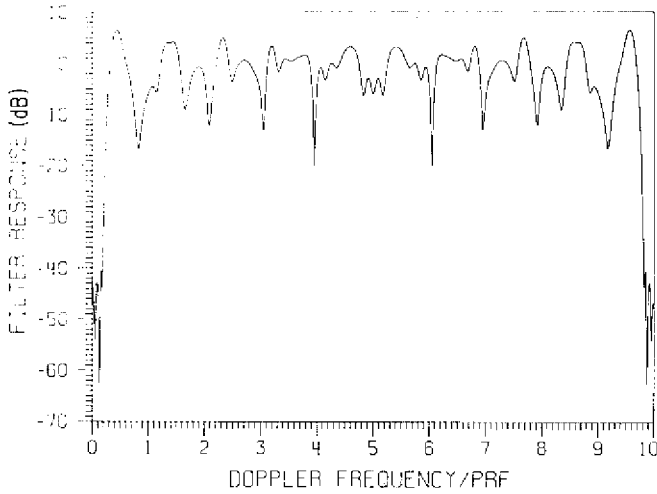
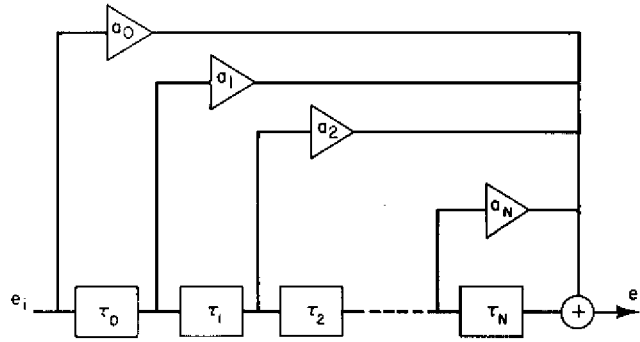
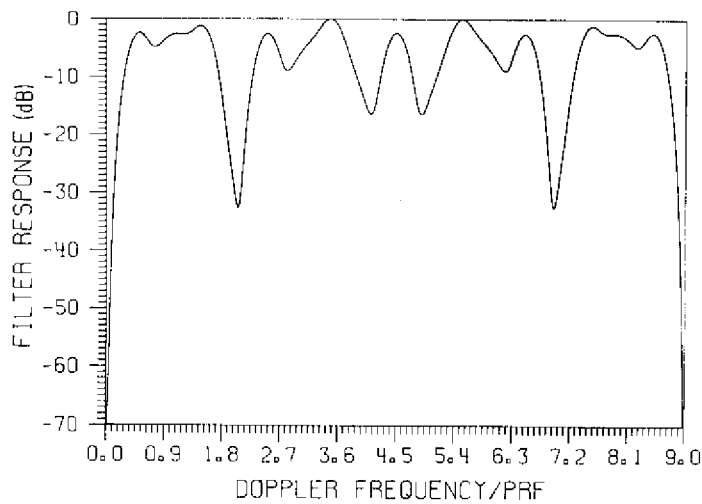


Fig. 12 — Frequency response for a seven-pulse staggered-PRF MTI filter.  
 (From Hsiao and Kretschmer, *Radio and Electronic Engineer* **43**, 689-693 (1973), courtesy of the Institution of Electronic and Radio Engineers.)

Fig. 13 — Target-signal gain function of a dual-frequency MTI system with  $r = 0.89$ . (From J. K. Hsiao, *Radio and Electronic Engineer* **45**, 351-356 (1975), courtesy of the Institution of Electronic and Radio Engineers.)



## Doppler Processing

An MTI canceler provides near optimal target detection in clutter but provides little or no improvement against receiver noise. McAulay\* formulated the problem as a classical detection problem and showed that the optimal detector could be structured approximately as an MTI canceler followed by a narrow-band doppler filter bank. This structure has the practical advantage of greatly reducing the dynamic range required at the input of the filter bank. In this configuration, the MTI canceler provides improvement against clutter, and the doppler filter bank provides improvement against noise.

The moving-target detector (MTD), developed by Lincoln Laboratory†‡ for the FAA, uses this type of processing. During 1976 the MTD was tested with a modified FPS-18 radar at the FAA facility in Atlantic City, N.J. The modified FPS-18 radar is an S-band radar instrumented to 48 n.mi. The range cell is approximately 1/16 n.mi., the beamwidth is 1.5°, the scan rate is 15 rpm, and 20 pulses are returned as the radar sweeps past the target.

A block diagram of the MTD signal processor is shown in Fig. 14. An azimuth cell is defined as a half beamwidth (0.75°) and contains ten pulses, with the time lapse for the ten pulses being referred to as a coherent processing interval (CPI). In a CPI the ten pulses are passed through a three-pulse MTI canceler, and the eight output pulses (two pulses are needed to load the MTI) serve as an input to an eight-point FFT, the points being weighted to provide low filter sidelobes. The radar PRF is changed from 1000 pps to 1150 pps on alternate CPIs to avoid the blind-speed problem.

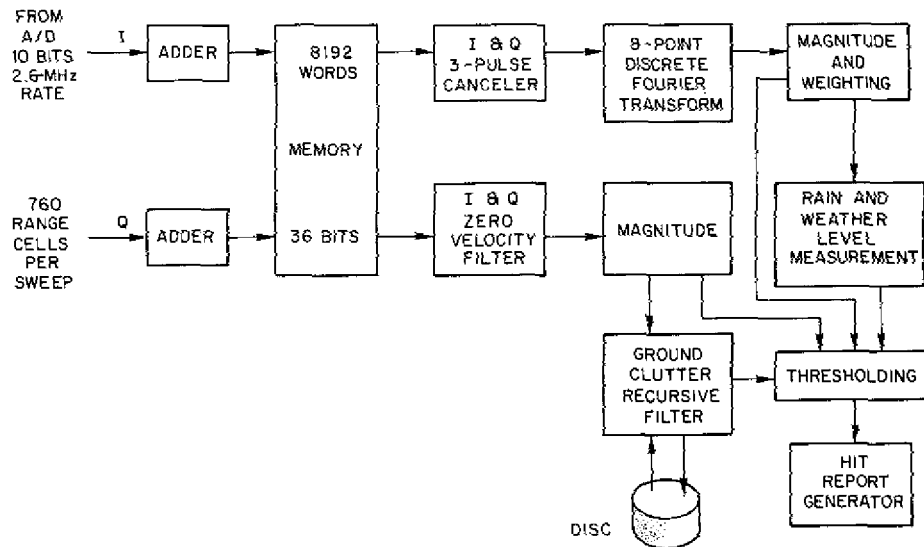


Fig. 14 — MTD signal processor

\*R. J. McAulay, Tech. Note 1972-14, Lincoln Laboratory, Mass. Inst. of Tech., 1972

†R. M. O'Donnell, C. E. Muehe, M. Labitt, W. H. Drury, and L. Cartledge, EASCON Convention Record 71-75, 1974

‡C. E. Muehe, L. Cartledge, W. H. Drury, E. M. Hofstetter, M. Labitt, P. B. McCorison, and V. J. Sferrino, Proc. IEEE 62, 716-723, (1974).

The  $2.9 \times 10^6$  range-azimuth-doppler cells ( $760 \times 360/0.75 \times 8$ ) are individually thresholded. In this process a clutter map is generated by weighting the radar return in the zero-doppler filter over the last eight scans (32 s) using a digital filter. Thus tangential targets having zero doppler can be detected if the target level exceeds the clutter-map level by a specified constant. That is, tangential targets can be detected in spotty ground clutter by using the principle of interclutter visibility\*. The thresholds for filters 2 through 6 are set using a mean-level threshold. Specifically the threshold for a given-number filter is based† on the average return in the given-number filter from the range cells  $\leq 1/2$  n.mi. (eight cells) on either side of the test cell. Since clutter spills over into filters 1 and 7, two thresholds are generated for these filters. One threshold is based on the map, a second threshold is based on the mean level over a range interval, and the higher of the two thresholds is used.

The MTD represents a great improvement in signal processing for FAA air-surveillance radars. A good match of processor to radar has been designed, and component technology has made the processing practical to implement. Presently, a second-generation MTD is being designed. This MTD uses no MTI, but rather each filter is optimized to obtain the maximum signal-to-clutter-plus-noise ratio for an assumed clutter spectrum.

### Noncoherent Moving-Target Indicators

Noncoherent MTIs are described in Skolnik's *Introduction to Radar Systems*‡ and *Radar Handbook*.§ They differ from coherent MTI by not using an internal coherent reference source but rather mixing the received signal with itself. Thus, when both clutter and a target are present, the beat between them yields a return at the target doppler. On the other hand, when only a target is present, the signal return is at zero doppler and cannot be detected. Consequently, for noncoherent MTI to be useful, gating circuitry is required for passing the noncoherent MTI output when clutter is present and passing the regular video when clutter is not present. Generally fringe areas cause major problems for the gating circuitry, making performance unacceptable.

A different kind of noncoherent MTI has been made possible by high-power microwave sources.# Lewis and Cantrell\*\* propose transmitting a short pulse and subtracting successive noncoherent pulses. This is similar to an area MTI discussed in *Introduction to Radar Systems*,‡ except that the short pulse enables the subtraction to be made on a pulse-to-scan pulse rather than a scan-to-scan basis. Thus, with a 1 ns pulse and a PRF of 200 pps, all moving targets above 60 knots can be detected; that is, there are no blind speeds.

\*D. K. Barton and W. W. Shrader, EASCON Conv. Record 294-297, 1969.

†Details about various thresholding techniques can be found in the section on noncoherent processing

‡M. I. Skolnik, *Introduction to Radar Systems*, McGraw-Hill, New York, 1962.

§M. I. Skolnik, editor *Radar Handbook*, McGraw-Hill, New York, 1970.

#V. L. Granatstein, P. Sprangle, M. Herndon, R. K. Parker, and S. P. Schlesinger, *J. Applied Physics* **46**, 3800-3805 (1975).

\*\*B. L. Lewis and B. H. Cantrell, "Short Pulse Noncoherent MTI", patent application, Navy Case 60372, NRL, Nov. 1975.

## NONCOHERENT DETECTION

The earliest noncoherent signal processing was performed by radar operators using visual inputs from PPIs and A-scopes. Although operators can perform this detection task accurately, operators are easily saturated and become quickly fatigued. To remedy this situation and to provide quick reaction times, automatic detection and tracking (ADT) systems have become quite popular during the 1970s. The statistical framework necessary for the development of ADT was introduced to the radar community in the 1940s by Marcum\*, and later Swerling† extended the work to fluctuating targets. They investigated many of the statistical problems associated with the *noncoherent detection of targets in Rayleigh noise*. Their most important result was the generation of curves of probability of detection ( $P_D$ ) versus signal-to-noise ratio (S/N) for a detector which sums  $N$  enveloped detected samples (either linear or square law) under the assumption of equal signal amplitudes. However, in a search radar, as the beam sweeps over the target, the returned signal amplitude is modulated by the antenna pattern. Many authors investigated various detectors (weightings), comparing detection performance and angular estimation results to the optimal values. The detectors investigated included the moving window, feedback integrator, two-pole filter, binary integrator, and batch processor.

In the original work on these detectors, the environment was assumed known and homogeneous, so that fixed thresholds could be used. However a realistic environment, containing land, sea, and rain for example, will cause an exorbitant number of false alarms for a fixed threshold system. Two approaches, *adaptive thresholding* and *nonparametric* detectors, have been used to solve the false-alarm problem. Both solutions are based on the assumption that homogeneity exists in a small region about the range cell that is being tested. The adaptive thresholding method assumes that the noise density is known except for a few unknown parameters. The surrounding reference cells are then used to estimate the unknown parameters, and a threshold based on the estimated density is obtained. *Nonparametric detectors* obtain a constant false-alarm rate (CFAR) by ranking the test sample with the reference cells. Under the hypothesis that all the samples (test and reference) are independent samples from an unknown density function, the test sample has a uniform density function; consequently a threshold which yields CFAR can be set.

### Classical Theory

The radar detection problem is a binary-hypothesis-testing problem:

$H_0$ : no target present

or

$H_1$ : target present.

Many criteria can be used to solve this problem, but the most appropriate for radar is the Neyman-Pearson‡ criterion. This criterion maximizes  $P_D$  for a given probability of false alarm

\*J. I. Marcum, IRE Trans. Information Theory 6, 59-267 (1960).

†P. Swerling, IRE Trans. Information Theory 6, 269-308 (1960).

‡J. Neyman and E. S. Pearson, Biometrika 20A, 175-240, 263-294 (1928).

$(P_{fa})$  by comparing the likelihood ratio ( $L$ ) to an appropriate threshold  $T$ . A target is declared present if

$$L(x_1, \dots, x_n) = \frac{p(x_1, \dots, x_n | H_1)}{p(x_1, \dots, x_n | H_0)} \geq T, \quad (45)$$

where  $p(x_1, \dots, x_n | H_1)$  and  $p(x_1, \dots, x_n | H_0)$  are the joint densities of the  $n$  samples under the conditions of target presence and target absence respectively. For a linear envelope detector and white Gaussian noise the samples have a Rayleigh density under  $H_0$  and a Ricean density under  $H_1$ , and the likelihood detector reduces to

$$\prod_{i=1}^n I_0 \left( \frac{A_i x_i}{\sigma^2} \right) \geq T, \quad (46)$$

where  $I_0$  is the Bessel function of zero order. For equal-amplitude ( $A_i = A$ ) small signal pulses ( $A_i \ll \sigma$ ), the detector reduces to the square-law detector:

$$\sum_{i=1}^n x_i^2 \geq T. \quad (47)$$

This detector and the linear detector were first studied by Marcum\* and were studied in succeeding years by numerous people. The most important facts concerning these detectors are the following:

- The detection performances of the linear and square-law detectors are similar and are close to the performance of the optimal detector.\*

- Since the signal return of a scanning radar is modulated by the antenna pattern, only 0.84 of the pulses between the half-power points should be integrated, and the antenna beam-shape factor (ABSF) is 1.6 dB.† The ABSF is the number by which the midbeam S/N must be reduced so that the detection curves generated for equal signal amplitudes can be used for the scanning radar.

- The collapsing loss for the linear integrator can be much greater than the loss for a square-law integrator.‡ The collapsing loss is the additional signal required to maintain the same  $P_D$  and  $P_{fa}$  when unwanted noise samples along with the desired signal-plus-noise samples are integrated.

Most signal processors are required not only to detect targets but to make angular estimates of the azimuth position of the target. Swerling§ calculated the standard deviation of the optimal estimate by using the Cramer-Rao lower bound. The results are shown in Fig. 15, where a normalized standard deviation is plotted against S/N per pulse. This result holds for a moderate or large number of pulses integrated, and the optimal estimate involves finding the location where the correlation of the returned signal and the derivative of the antenna pattern is zero. Although this estimate is rarely implemented, its performance is approached by simple

\*J. I. Marcum, IRE Trans. Information Theory 6, 59-267 (1960).

†L. V. Blake, Proc. IRE 41, 770-774 (1953).

‡G. V. Trunk, Proc. IEEE 60, 743-744 (1972).

§P. Swerling, Proc. IRE 44, 1146-1155 (1956).

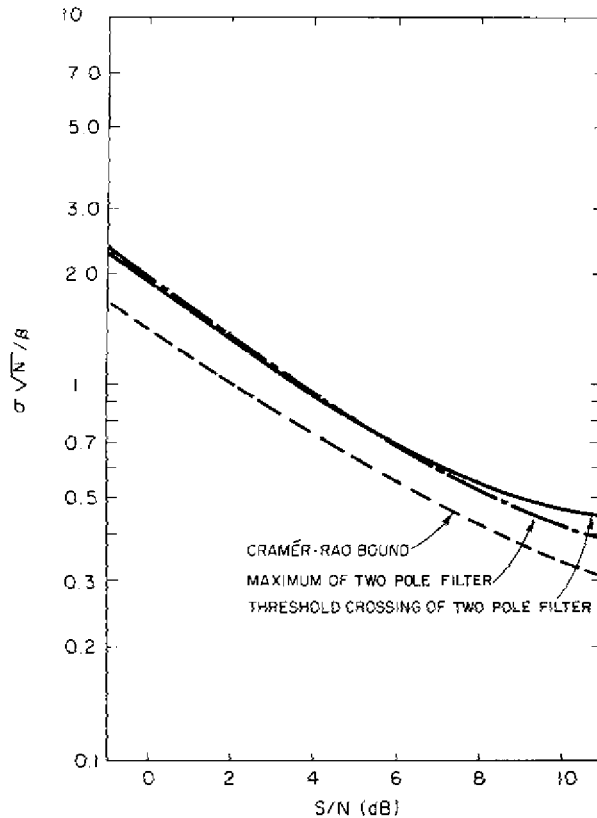


Fig. 15 — Comparison of angular estimates with the Cramer-Rao lower bound. In the ordinate expression,  $\sigma$  is the standard deviation of the estimation error and  $N$  is the number of pulses within the 3-dB beamwidth, which is  $2\beta$ .

estimates, such as the maximum-value and threshold-crossing procedures, as can be seen in Fig. 15.

### Integrators

Almost all signal processors use linear rather than square-law detectors, since a linear detector is easily built by using a matched filter and a half-wave rectifier followed by a low-pass filter. However many different integrators are used to accumulate the linear-envelope-detected pulses. A few of the most common integrators are shown in Fig. 16. Some advantages and disadvantages of these integrators are as follows.\*†‡

#### *Moving window*

The moving window performs a running sum of  $N$  pulses; as the latest pulse is added to the sum, the pulse that is  $N$  PRFs in the past is subtracted from the sum. The detection performance of this detector is only 0.5 dB worse than the optimal detector which weights the returned signal by the fourth power of the voltage antenna pattern. The angular estimate is ob-

\*D. S. Palmer and D. C. Cooper, *IEEE Trans. Information Theory* **IT-10**, 296-302 (1964).

†G. M. Dillard, *IEEE Trans. Information Theory* **IT-13**, 2-6 (1967).

‡B. H. Cantrell and G. V. Trunk, *IEEE Trans. Aerospace and Electronic Systems* **AES-9**, 649-653 (1973).

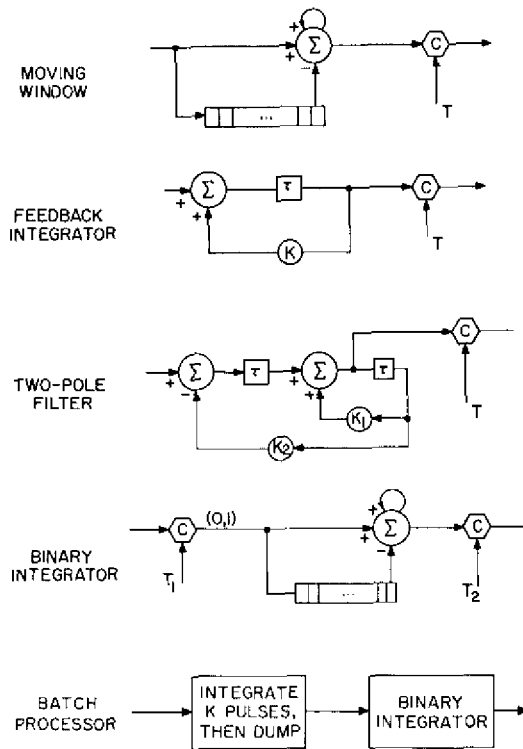


Fig. 16 - Common integrators

tained by either taking the maximum value of the running sum or taking the midpoint between the first and last crossing of the detection threshold. Both methods have a bias of  $N/2$  pulses which is easily corrected. The standard deviation of the estimation error of both estimators is about 20% higher than the Cramer-Rao lower bound. The major disadvantage of this detector is that the last  $N$  pulses for each range cell must be saved. For radars with large beamwidths and thus many pulses, the moving window requires extensive hardware. However with the lower cost and size of memory this disadvantage is rapidly disappearing.

*Feedback integrator*

The amount of storage required can be reduced significantly by using a feedback integrator, which requires the storage of only one number. Although the feedback integrator applies an exponential weighting into the past, its detection performance is only 1 dB less than the optimal integrator. Unfortunately difficulties are encountered when using the feedback integrator to estimate the azimuth position. The threshold-crossing procedure yields estimates only 20% greater than the lower bound, but the bias is a function of  $S/N$  and must be estimated. On the other hand the maximum value, although having a constant bias, has estimates which are 100% greater than the lower bound. This author's opinion is that this detector has limited utility.

*Two-pole filter*

The two-pole filter requires the storage of an intermediate calculation in addition to the integrated output. However with this rather simple device a weighting pattern similar to the antenna pattern can be obtained; consequently good performance would be expected. The detection performance is within 0.15 dB of the optimal detector, and its angular estimates are about 20% greater than the Cramer-Rao lower bound. If the desired number of pulses integrated is changed (because of change in rotation of the radar or use of another radar), it is necessary to change only the feedback values  $K_1$  and  $K_2$ . Their optimal values are set by

$$K_1 = 2 e^{-\psi \omega_d \tau / \sqrt{1 - \psi^2}} \cos(\omega_d \tau) \quad (48)$$

and

$$K_2 = e^{-2\psi \omega_d \tau / \sqrt{1 - \psi^2}}, \quad (49)$$

where  $\psi = 0.63$ ,  $N\omega_d \tau = 2.2$ , and  $N$  is the number of pulses between the 3-dB points of the antenna.

*Binary Integrator*

The binary integrator is also known as the dual-threshold detector,  $M$ -out-of- $N$  detector, or rank detector. The input samples are quantized to 0 or 1 depending on whether or not they are less than a threshold  $T_1$ . The last  $N$  zeros and ones are summed and compared to a second (detection) threshold  $T_2 = M$ . The detection performance of this detector is 2 dB less than the moving-window integrator because of the hard limiting of the data, and the angular estimation error is 25% greater than the Cramer-Rao lower bound. This detector is used because it is easily implemented, it ignores interference spikes which cause trouble with integrators that directly use signal amplitude, and it works extremely well when\*† the noise has a non-Rayleigh density.

A comparison of the binary integrator (three out of three), the median detector (two out of three), and the mean detector (moving window) in log-normal interference is shown in Fig. 17. The optimal binary integrator is much better than straightforward integration. The optimal values for the second threshold were found by Schwartz‡ for Rayleigh interference and by Schleher§ for log-normal interference.

*Batch Processor*

The batch processor is used when there are a large number of pulses in the 3-dB beamwidth. If  $KN$  pulses are in the 3-dB beamwidth,  $K$  pulses are summed and either a 0 or 1 is declared depending on whether or not the sum is less than a threshold  $T_1$ . The last  $N$  zeros and ones are summed and compared to a second threshold  $M$ .

\*D. C. Schleher, IEEE 1975 International Radar Conf., 262-267, 1975.

†G. V. Trunk, "Non-Rayleigh Sea Clutter: Properties and Detection of Targets," NRL Report 7986, June 1976.

‡M. Schwartz, IEEE Trans. Information Theory 2, 135-139 (1956).

§D. C. Schleher, IEEE 1975 International Radar Conf., 262-267, 1975.

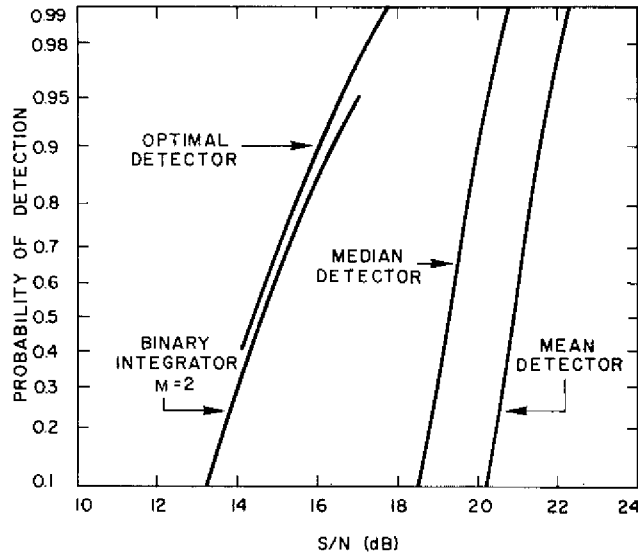


Fig. 17 — Comparison of various detectors in log-normal interference ( $N = 3$ ,  $P_{fa} = 10^{-6}$ )

The batch processor, like the binary integrator, is easily implemented, ignores interference spikes, and works extremely well when the noise has a non-Rayleigh density, but furthermore in comparison with the binary integrator the batch processor requires less storage, detects better (less than 2 dB from moving window), and estimates angles more accurately.

The batch processor has been implemented by the Applied Physics Laboratory\* of Johns Hopkins University with great success. To obtain a more accurate azimuth estimate, they use

$$\hat{\theta} = \frac{\sum A_i \theta_i}{\sum A_i}, \quad (50)$$

where  $A_i$  are the amplitudes of the sums greater than  $T_1$  and  $\theta_i$  are the corresponding antenna azimuth angles. When many pulses are on target ( $N > 20$ ), this detector is generally favored by this author.

### False Alarms

If fixed thresholds are used with the previously discussed integrators, the detectors will saturate the tracking computer associated with the system and disrupt the system. Three important facts should be remembered:

- It makes little sense to have an automatic detection system without an associated tracking system;
- The sensitivity of the detector should be as high as possible without saturating the tracking computer;

\*"Radar Processing Subsystem Evaluation", Vol. I, APL Report FP8-T-013, Nov. 1975.

REPORT DOCUMENTATION PAGE		READ INSTRUCTIONS BEFORE COMPLETING FORM
1. REPORT NUMBER NRL REPORT 8117	2. GOVT ACCESSION NO.	3. RECIPIENT'S CATALOG NUMBER
4. TITLE (and Subtitle) SURVEY OF RADAR SIGNAL PROCESSING		5. TYPE OF REPORT & PERIOD COVERED Final Report on one phase of a continuing NRL Problem
		6. PERFORMING ORG. REPORT NUMBER
7. AUTHOR(s) G. V. Trunk		8. CONTRACT OR GRANT NUMBER(s)
9. PERFORMING ORGANIZATION NAME AND ADDRESS Naval Research Laboratory Washington, D. C. 20375		10. PROGRAM ELEMENT, PROJECT, TASK AREA & WORK UNIT NUMBERS NRL Problem R02-97 Program Element 61153N Project RR021-05-41
11. CONTROLLING OFFICE NAME AND ADDRESS Department of the Navy Office of Naval Research Arlington, Va. 22217		12. REPORT DATE June 21, 1977
		13. NUMBER OF PAGES 48
14. MONITORING AGENCY NAME & ADDRESS (if different from Controlling Office)		15. SECURITY CLASS. (of this report) Unclassified
		15a. DECLASSIFICATION/DOWNGRADING SCHEDULE
16. DISTRIBUTION STATEMENT (of this Report) Approved for public release; distribution unlimited		
17. DISTRIBUTION STATEMENT (of the abstract entered in Block 20, if different from Report)		
18. SUPPLEMENTARY NOTES		
19. KEY WORDS (Continue on reverse side if necessary and identify by block number)		
Coherent processing	Noncoherent detection	Tracking filters
Sidelobe cancelers	Integrators	Correlation logic
Adaptive radars	Adaptive thresholding	Radar integration
MTI	Nonparametric detectors	
Doppler processing	Track-while-scan	
20. ABSTRACT (Continue on reverse side if necessary and identify by block number)		
<p>During the last decade, considerable progress has been made in radar signal processing, and this report states its present status. The three broad areas of coherent processing, noncoherent detection, and track-while-scan systems are discussed.</p> <p>Specifically, in the area of coherent processing the subjects of sidelobe cancelers, adaptive radars, MTIs, and doppler processing are discussed. In the adaptive processing area, both the maximum signal-to-noise and least mean-square methods are described, and special emphasis is given to</p> <p style="text-align: right;">(Continued)</p>		

DD FORM 1473  
1 JAN 73EDITION OF 1 NOV 65 IS OBSOLETE  
S/N 0102-LF-014-6601

- False alarms and false targets are not a problem if they are removed by the tracking computer. Tracking (scan-to-scan processing) is the only way to remove stationary point clutter or target MTI residues.

One can reduce the number of false alarms with a fixed-threshold system by setting a high threshold, but this would reduce sensitivity in regions of low-noise (clutter) return. A detector is required which will detect a target when it has a higher return than its immediate background. Two such types of detectors are adaptive-thresholding and nonparametric detectors. Both of these detectors assume that the samples in the range cells surrounding the test cell (called reference or neighboring cells) are independent and identically distributed; furthermore it is usually assumed that the time samples are independent. Both detectors test whether the test cell has a return sufficiently larger than the reference cells. A survey of CFAR procedures can be found in Hansen\*.

#### *Adaptive Thresholding*

The basic assumption of the adaptive-thresholding technique is that the noise density is known except for a few unknown parameters. The surrounding reference cells are used to estimate the unknown parameters, and a threshold based on the estimated density is then obtained. The simplest adaptive detector is the cell-averaging CFAR investigated by Finn and Johnson†. If the noise has a Rayleigh density, only the parameter  $\sigma$  needs to be estimated, since the mean of a Rayleigh distribution is  $\sigma\sqrt{\pi}/2$  and the variance is  $\sigma^2(2v-\pi/2)$ . Thus, by estimating the mean, one obtains an estimate  $\hat{\sigma}$  which can be used to set a threshold  $T$  to yield the desired  $P_{fa}$ . However, since  $T$  is set by an estimate  $\hat{\sigma}$ , it must be slightly larger than the threshold one would use if  $\sigma$  were known a priori. The raised threshold causes a loss in target sensitivity and is referred to as a CFAR loss. This loss has been calculated by Mitchell and Walker‡, and some results are summarized in Table 2. As can be seen, for a small number of reference cells, the loss is large because of the poor estimate of  $\sigma$ .

This thresholding technique is more effective in maintaining CFAR when it is applied to the binary integrator or batch processor, as shown in Fig. 18. This is because when the number of pulses integrated by the binary integrator is moderate, the  $P_{fa}$  on a single pulse is rather large; for example  $P_{fa} = 0.1$  for a single pulse yields  $P_{fa} = 10^{-3}$  for a seven-out-of-ten integrator. Thus, since most non-Rayleigh densities are Rayleigh-like to the 10th percentile, this type of processor will maintain a low  $P_{fa}$  in most non-Rayleigh environments. This demonstrates a general rule: to maintain a low  $P_{fa}$  in various environments, adaptive thresholding should be placed in front of the integrator. For any noise distribution, CFAR can be maintained by counting the number of ones out of the comparator per scan and using this number to control  $K$ ; that is, if the number is too large,  $K$  is increased.

Front-end thresholding, which maintains amplitude information by dividing the average reference value into the test cell, was investigated by Hansen and Ward§ and is shown in Fig. 19. This type of processing is especially effective when there is strong interference which is variable on a pulse-to-pulse basis.

\*V. G. Hansen, IEEE International Conference on Radar — Present and Future, 325-332, 1973.

†H. M. Finn and R. S. Johnson, RCA Review 29, 414-464 (1968).

‡R. L. Mitchell and J. K. Walker, IEEE Trans. Aerospace and Electronic Systems AES-7, 671-676 (1971).

§V. G. Hansen and H. R. Ward, IEEE Trans. Aerospace and Electronic Systems 8, 648-652 (1972).

Table 2 — CFAR Loss for  $P_{fa} = 10^{-6}$  and  $P_D = 0.9$

Number of Pulses Integrated	Loss for Various Numbers of Reference Cells (dB)					
	1	2	3	5	10	$\infty$
1	-	-	15.3	7.7	3.5	0
3	-	7.8	5.1	3.1	1.4	0
10	6.3	3.3	2.2	1.3	0.7	0
30	3.6	2.0	1.4	1.0	0.5	0
100	2.4	1.4	1.0	0.6	0.3	0

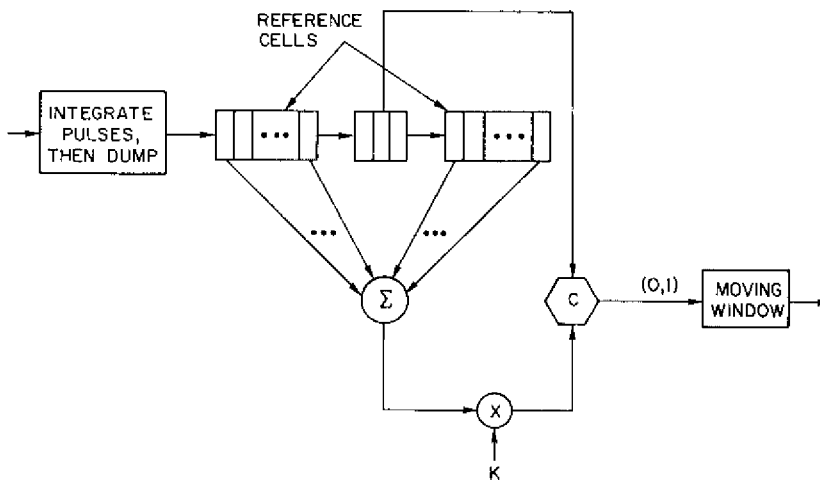


Fig. 18 — Cell-averaging CFAR implemented with the batch processor

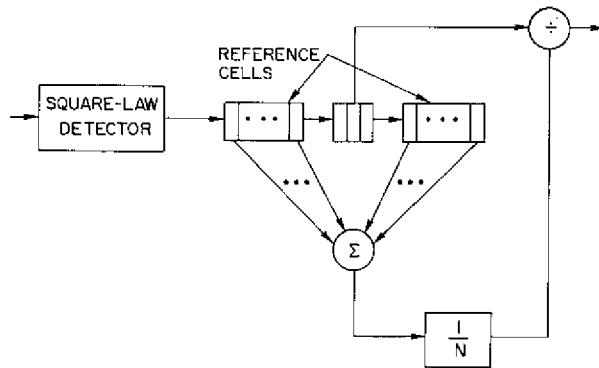


Fig. 19 — Front-end cell-averaging CFAR receiver

When the noise has a non-Rayleigh density, such as the chi-square density or log-normal density, two parameters must be estimated, and the adaptive detector is more complicated. If several pulses are integrated with any of the amplitude integrators, the integrated output will be approximately Gaussian distributed. Then the two parameters which must be estimated are the mean and the variance. These estimates are given by

$$\bar{X} = \frac{1}{N} \sum_i x_i, \quad (51)$$

and

$$\hat{\sigma}^2 = \frac{1}{N} \sum_i x_i^2 - \bar{X}^2 \quad (52)$$

where the summation is over the  $N$  range cells surrounding the test cell.

When successive pulses in the same range cell are correlated (as with returns from rain or sea clutter), many false alarms will occur if only the mean value (51) is estimated. A threshold of the form

$$T = \bar{X} + K\hat{\sigma} \quad (53)$$

will provide a low  $P_{fa}$  for the amplitude integrators: moving window, feedback integrator, and two-pole filter. Nothing can be done to the binary integrator to yield a low  $P_{fa}$  in correlated noise; thus it should not be used in this situation. On the other hand, if the correlation time is less than a batching interval, the batch processor will yield a low  $P_{fa}$  without modifications.

#### *Nonparametric Detectors*

The most common way nonparametric detectors obtain CFAR is by ranking the test sample with the reference cells. Under the hypothesis that all the samples are independent samples from an unknown density function, the test sample has a uniform density function. For instance, with reference to the rank detector in Fig. 20, the test cell is compared to 15 of its neighbors. Since in the set of 16 samples the test sample has equal probability of being the smallest sample (rank = 0 or equivalently any other rank), the probability that the test sample takes on values 0, 1, ..., 15 is 1/16. A simple rank detector\* can be constructed by comparing the rank (number of reference cells that the test cell exceeds) to a threshold  $K$ ; and the output is 1 if the rank is larger and 0 otherwise. The zeros and ones are summed in a moving window. This detector incurs a CFAR loss of about 2 dB and is extremely effective, if the time samples are independent. Only certain values of  $P_{fa}$  can be obtained. Thus, if the number of pulses integrated is small, low  $P_{fa}$  values cannot be obtained.

If the time samples are dependent, the rank detector will not yield CFAR. A modified rank detector, called the modified generalized sign test† (MGST) is an attempt to maintain a low  $P_{fa}$  and is that shown in Fig. 20. This detector can be divided into three parts: a ranker, an integrator (in this case a two-pole filter), and a thresholding device. A target is declared when the integrated output exceeds two thresholds. The first threshold is fixed (equals  $\mu + T_1/K$  from Fig. 20) and yields CFAR when the reference cells are independent and identically distributed. The second threshold is adaptive and maintains a low  $P_{fa}$  when the

\*V. G. Hansen and B. A. Olsen, IEEE Trans. Aerospace and Electronic Systems 4, 942-950 (1971).

†G. V. Trunk, B. H. Cantrell, and F. D. Queen, IEEE Trans. Aerospace and Electronic Systems 10, 574-582 (1974).

20. ABSTRACT (Continued)

the problem of convergent rate. The moving-target detector (MTD) is used as an example of doppler processing.

In the area of noncoherent detection, various integrators are discussed. Among these are the moving window, feedback integrator, two-pole filter, binary integrator, and batch processor. Methods of obtaining a constant false-alarm rate using either adaptive thresholding or nonparametric detectors are also considered.

A general outline of a track-while-scan system is considered first. Then, detailed discussions of the tracking filter, maneuver-following logic, track initiation, and correlation logic are presented. Finally, methods of integrating data from several radars are discussed.

## CONTENTS

INTRODUCTION .....	1
COHERENT PROCESSING .....	1
Sidelobe Cancelers .....	2
Adaptive Arrays and Radars .....	6
Moving-Target Indicators .....	14
Doppler Processing .....	18
Noncoherent MTI Indicators .....	19
NONCOHERENT DETECTION .....	20
Classical Theory .....	20
Integrators .....	22
Moving Window .....	22
Feedback Integrator .....	23
Two-Pole Filter .....	24
Binary Integrator .....	24
Batch Processor .....	24
False Alarms .....	25
Adaptive Thresholding .....	26
Nonparametric Detectors .....	28
Sequential Detectors .....	30
TRACKING SYSTEM .....	31
System Outline .....	32
Tracking Filters .....	33
Maneuver-Following Logic .....	35
Track Initiation .....	38
Correlation Logic .....	38
Radar Integration .....	41
CONCLUDING REMARKS .....	44

# SURVEY OF RADAR SIGNAL PROCESSING

## INTRODUCTION

During the last decade considerable progress has been made in radar signal processing. This progress is directly traceable to the lowered cost and increased speed of digital hardware and computers and to more sophisticated techniques in adaptive processing and tracking systems.

This survey of radar signal processing will neglect waveform design and include the track-while-scan systems. Waveform design will be neglected because it has received considerable attention elsewhere, with the books of Rihaczek\* and Cook and Bernfeld† covering the subject in detail. On the other hand, although track-while-scan systems properly fall under the heading of radar data processing, it does not make sense to have an automatic detection system unless it is accompanied by a tracking system. Therefore, since tracking is a necessary part of the entire system, the survey will include it.

Thus this survey of radar signal processing will consider the three broad areas of coherent processing (processing of amplitude and phase), noncoherent processing (processing of amplitude), and track-while-scan systems. The subjects will be discussed in the same order as the radar signal passes through the radar system. Specifically, in the area of coherent processing the subjects of sidelobe cancelers, adaptive antennas, and MTIs (moving-target indicators) will be covered. In the area of noncoherent detection, methods of obtaining a constant false-alarm rate (CFAR) using either adaptive thresholding or nonparametric detectors will be emphasized. The section on the tracking system will cover the tracking filter, correlation logic, track initiations, maneuver-following logic, and a basic overview of an entire tracking system.

## COHERENT PROCESSING

In the area of coherent processing, adaptive processing will receive considerable attention. There are two approaches to adaptive processing: the method of maximum signal-to-noise ratio (S/N) due to Howells‡ and Applebaum§ and the least-mean-square method (LMS) due to Widrow and Hoff#. The two methods, although appearing quite different, yield almost equivalent results. So that both methods will be presented, the LMS method will be used during discussion of sidelobe cancelers, and the method of maximum S/N will be used during discussion of adaptive arrays and radars. For adaptive radars special consideration will be given to

---

\*A. W. Rihaczek, *Principles of High-Resolution Radar*, McGraw-Hill, New York, 1969.

†C. E. Cook and M. Bernfeld, *Radar Signals, An Introduction to Theory and Application*, Academic Press, New York, 1967.

‡P. W. Howells, IEEE Trans. Antennas and Propagation AP-24, 575-584 (1976).

§S. P. Applebaum, IEEE Trans. Antennas and Propagation AP-24, 585-598 (1976).

#B. Widrow and M. E. Hoff, IRE WESCON Conv. Rec., 96-104, 1960.

the problem of convergent rate. Finally, MTIs will be discussed and the moving-target-detector (MTD) system will be used as an example of doppler processing.

### Sidelobe Cancelers

The basic idea of a sidelobe canceler (a device that attempts to eliminate interference entering through the antenna sidelobes) is shown in Fig. 1. The signal  $S$  of interest enters through the main lobe of the antenna, and the jamming (interfering signal), which is much stronger than the signal of interest, enters through the sidelobe of the main antenna. The auxiliary antenna is an omnidirectional antenna, and it will be assumed that the signal entering the omnidirectional antenna is much smaller than the jamming  $J_a$  and can be neglected, since the signal and jamming now have the same antenna gain. (The treatment of the signal in the auxiliary channel can be found in Widrow et al.)\* The adaptive filter produces an output  $Y$  which is as close as possible to the input jamming  $J$ . The filter output is then subtracted from the main input, producing an output  $Z = S + J - Y$ . If the filter output is an exact replica of  $J$ , the output is the desired signal  $S$ .

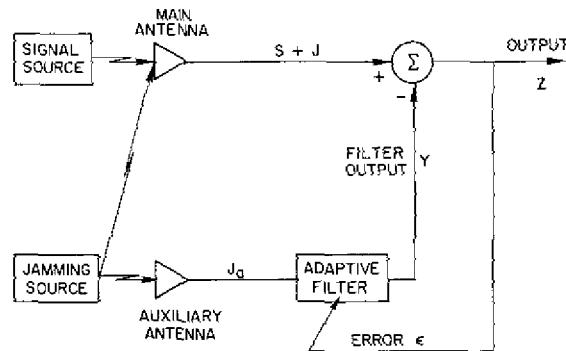


Fig. 1 — Concept of adaptive noise canceling

The filter is controlled by adjusting its parameters to minimize the output power. To show that this minimization will force  $Y$  to be a replica of  $J$ , a development in Widrow et al.\* is repeated. First, assume  $S$ ,  $J$ , and  $J_a$  are zero-mean random variables,  $S$  is uncorrelated with  $J$  and  $J_a$ , and  $J_a$  (and hence  $Y$ ) is correlated with  $J$ . The expected output power is

$$E\{Z^2\} = E\{S^2\} + E\{(J - Y)^2\} + 2E\{S(J - Y)\} = E\{S^2\} + E\{(J - Y)^2\}. \quad (1)$$

Adjusting the filter to minimize  $E\{Z^2\}$  is equivalent to minimizing  $E\{(J - Y)^2\}$ , since  $Y$  is uncorrelated with  $S$ ; that is,  $Y$  is the best least-squares estimate of the jamming  $J$ . Furthermore, since  $Z - S = J - Y$ , minimizing  $E\{(J - Y)^2\}$  causes  $Z$  to be the best least-squares estimate of the signal  $S$ .

The adaptive filter for obtaining a least-squares estimate of a desired signal  $S$  can be described by a weighting vector  $W$ , where  $W^T = (W_1, W_2, \dots, W_n)$  and  $T$  denotes the transpose, operating on the input  $J_a = X$ ,  $X^T = (x_1, \dots, x_n)$ . Thus the filter output is

$$Y = X^T W, \quad (2)$$

\*B. Widrow, J. R. Glover, Jr., J. M. McCool, J. Kaunitz, C. S. Williams, R. H. Hearn, J. R. Zeidler, E. Dong, Jr., and R. C. Goodlin, Proc. IEEE 63, 1692-1716 (1975).

and the error, defined as the difference between the input signal and the filter output, is

$$\epsilon = S + J - X^T W. \quad (3)$$

The least-mean-square (LMS) adaptive filter adjusts the weighting vector  $W$  to minimize the mean-square error. The squared error is

$$\epsilon^2 = (S + J)^2 - 2(S + J)X^T W + W^T X X^T W. \quad (4)$$

Taking the expected value of (4), letting the vector  $P$  be the crosscorrelation between  $J$  and  $X$  ( $P = E\{JX\}$ ), and letting the matrix  $K$  be the covariance matrix of  $X$  ( $K = E\{XX^T\}$ ), one obtains

$$E\{\epsilon^2\} = E\{S^2\} + E\{J^2\} - 2P^T W + W^T K W. \quad (5)$$

To find the minimum of (5) with respect to  $W$ , the gradient  $\nabla$  of (5) is set to zero, yielding the optimal weight vector

$$W = K^{-1} P. \quad (6)$$

The LMS adaptive algorithm is an iterative method of finding an approximate solution to (6). The algorithm has the advantage of not requiring an explicit measurement of the correlation function or inversion of the covariance matrix. Specifically, the LMS algorithm uses the method of steepest descent to solve (6); that is, the next weight vector  $W_{j+1}$  is equal to the old weight vector plus a step in the direction of the negative gradient:

$$W_{j+1} = W_j - \mu \nabla_j. \quad (7)$$

The gradient of the squared error on the  $j$ th iteration is

$$\nabla_j = \nabla \epsilon_j^2 = \nabla (S + J - X_j^T W_j)^2 = -2\epsilon_j X_j. \quad (8)$$

Thus the next weight is given recursively by

$$W_{j+1} = W_j + 2\mu \epsilon_j X_j \quad (9)$$

and is known as the Widrow-Hoff LMS algorithm. The parameter  $\mu$  is a factor which controls the rate of convergence and the stability of the method. It has been shown\*† that (9) converges to the optimal solution as long as  $\mu$  is between zero and the reciprocal of the largest eigenvalue of the covariance matrix  $K$ . Shown in Fig. 2 is a typical learning curve and an average of 48 learning curves for the LMS algorithm. The average reveals the basic exponential nature of the learning curve. For the radar case  $X_j$  represents the sample from  $j$ th range cell; consequently the number of iterations corresponds to the number of range cells.

In principal, if the situation shown in Fig. 1 is correct (no uncorrelated noise in each channel and no signal in the auxiliary) the jamming can be completely canceled. However, if the situation is as shown in Fig. 3, total cancellation cannot be accomplished. Specifically, the performance of the canceler can be described by the ratio  $R$  of S/N at the output to S/N at the

\*B. Widrow, P. E. Mantey, L. J. Griffiths, and B. B. Goode, Proc. IEEE 55, 2143-2159 (1967).

†R. L. Riegler and R. T. Compton, Jr., Proc. IEEE 61, 748-758 (1973).

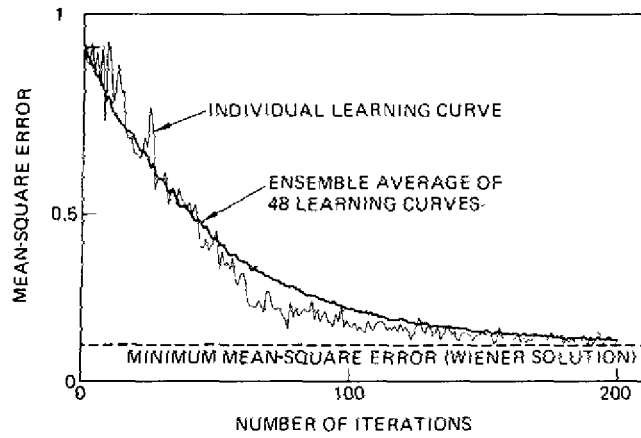


Fig. 2 — Typical learning curves for the LMS algorithm. (From) B. Widrow et al., Proc. IEEE 63, 1692-1716 (1975), courtesy of the Institute of Electrical and Electronics Engineers.)

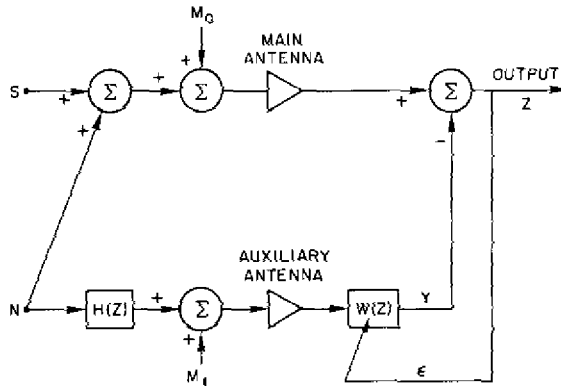


Fig. 3 — Adaptive noise canceller with correlated and uncorrelated noises in the main and auxiliary antennas

primary input (main antenna). Widrow et al.\* have shown that this ratio  $R$  for steady state (after convergence) can be expressed as

$$R = \frac{[A(z) + 1] [B(z) + 1]}{A(z) + A(z) B(z) + B(z)}, \quad (10)$$

where  $A(z)$  and  $B(z)$  are noise-to-noise ratios

$$A(z) = S_0(z)/S_n(z) \quad (11)$$

and

$$B(z) = S_1(z)/S_n(z) |H(z)|^2, \quad (12)$$

\*B. Widrow, J. R. Glover, Jr., J. M. McCool, J. Kaunitz, C. S. Williams, R. H. Hearn, J. R. Zeidler, E. Dong, Jr., and R. C. Goodlin, Proc. IEEE 63, 1692-1716 (1975).

in which  $S_0$ ,  $S_1$ , and  $S_n$  are the power density spectra of the noises  $m_0$ ,  $m_1$ , and  $n$  respectively and  $H(z)$  is the channel transfer function for the correlated noise (jamming). It is obvious from (10) that the cancellation is limited by the uncorrelated noise components in the primary and reference channels. When the jamming is much stronger than the uncorrelated noise components,  $A(z)$  and  $B(z)$  are small and

$$R \simeq \frac{1}{A(z) + B(z)}, \quad (13)$$

giving a large improvement in the output signal-to-jamming ratio. However the improvement indicated by (13) is rarely achieved in practice. Factors limiting performance include the finite time for the adaptive process, the presence of signal components in the auxiliary channel, multipath problems, and misadjustment caused by gradient estimation noise in the adaptive process.\* Furthermore, in theory  $N$  omnidirectional antennas (and associated cancellation loops) are needed to cancel  $N$  jammers. However, because of multipath propagation, the energy from a single jammer can enter the antenna from several directions and for all practical purposes appears to be from several jammers. Therefore in practice one requires several times as many cancellation loops as jammers.

Recently F. Kretschmer and B. Lewis† have developed an improved algorithm for simulation of the Applebaum-Howells adaptive loop and for use in adaptive processing. The LMS algorithm discussed above is given by

$$W_{j+1} = W_j + 2\mu\epsilon_j X_j. \quad (9)$$

This is commonly used to simulate and analyze the Applebaum-Howells adaptive loop in the form

$$W_{j+1} = kW_j + G(1 - k)\epsilon_j X_j^*, \quad (14)$$

where  $k = 1 - 1/\tau$ , with  $\tau$  being the filter smoothing constant, and  $G$  being the gain term. Thus in both algorithms the next weight is derived in terms of the present error and sample. Kretschmer and Lewis point out that for fast loops  $W_{j+1}$  as given by (9) and (14) is not the proper weight. Rather, for better cancellation and more realistic canceler loop simulation,  $W_{j+1}$  should be calculated from

$$W_{j+1} = W_j + 2\mu\epsilon_{j+1} X_{j+1}^*. \quad (15)$$

In effect, by using the sample  $X_j$  to calculate the weight  $W_{j+1}$ , a phase shift is introduced which can result in loop instability. Kretschmer and Lewis have shown (for the Applebaum-Howells application) that the stability condition of the LMS algorithm is

$$|G(1 - k)|X_j|^2 - k| < 1 \quad (16)$$

and that their improved algorithm is unconditionally stable.

Comparison of the LMS algorithm with the improved algorithm was made using computer simulations. Correlated Gaussian noise (mean = 0, variance = 2) was used as an input to the main and auxiliary channels of the sidelobe canceler. At the 250th range cell a constant signal at  $S/N = -20$  dB is introduced. The signal residue for both algorithms with canceler

\*B. Widrow, P. E. Mantey, L. J. Griffiths, and B. B. Goode, Proc. IEEE 55, 2143-2159 (1967).

†F. Kretschmer and B. L. Lewis, "An Improved Algorithm for Adaptive Processing," NRL Report 8084, Dec. 1976.